In-situ, Inc.
209 GRAND AVE., LARAMIE, WY 82070 (307) 742-8213
Telecopier (307) 742-8226
TWX 910 949-4944

Design Criteria for In-Situ Mining of Hard Rock Ore Deposits

by

C.R. McKee, R.H. Jacobson, S.C. Way
M.E. Hanson and K. Chong

Presented at the
2nd SME-SPE International
Solution Mining Symposium
November 18-20, 1981
Denver, CO.

Design Criteria for In-Situ Mining of Hard Rock Ore Deposits

1.0 Introduction

In-situ mining of hard rock deposits will only become successful as we understand the engineering parameters involved and the design limitations they impose. As recognized by Wadsworth[1] the most critical area is the enhancement of permeability in a hard rock mass. Along with creating permeability, the appropriate flow and fragment size conditions must be generated to insure economic rates of mineral recovery. In this article our interest is confined to true in-situ processes in which boreholes are drilled from the ground surface or a mine drift to deeper strata. We assume that fractures and permeability enhancement will be due to explosives detonated in boreholes. Other techniques such as hydraulic fracturing do not produce the necessary size distribution to promote economic extraction rates unless the medium is already highly fractured and interconnected.[2] Notable exceptions where hydraulic fracturing is applicable are many oil, gas and salt deposits. For many in-situ processes, an array of explosive charges offers the opportunity of creating a distribution of many fractures not achievable by other techniques. Such a situation would be suitable, for example, to in-situ mine hard rock gold, uranium, copper or oil shale deposits and may enhance oil and gas recovery in certain situations.

The purpose of our article is to review and extend the explosive permeability theory of McKee and Hanson[3,4,5] and to apply its results to derive design parameters suitable for in-situ mining.

2.0 Explosive Phenomenology

Direct observation of explosion phenomenology in earth media is limited to a few dynamic stress and velocity histories at selected points from the explosive source and postshot excavation of the region around the blast generated

cavity. Knowledge of the processes involved in the shock propagation and fracturing of the surrounding rock are deduced from numerical computer calculations. These models contain the basic physics and use medium property model parameters developed from laboratory measurements on small rock samples. The computer models have been verified by comparison with field data and the observations noted above. Agreement is good for final cavity size and peak stress and velocity vs. range (i.e., attenuation of the shock wave strength). Improvements in predictive capability are still needed for stress wave form and far field displacement.

To verify the theory developed later, we rely on post-shot permeability measurements taken around cavities formed by detonating chemical and nuclear explosives. Accordingly, we discuss each explosive type separately.

Detonation of a tamped chemical high explosive in a borehole deep below the ground surface results in a peak stress into the rock of slightly greater than 100 kbars which may vaporize the water in the rock for a few centimeters beyond the borehole wall.

Detonation of a nuclear explosive deep below the ground surface produces an extremely high temperature - high pressure spherical ball of plasma. A high intensity shock wave is generated, propagating into the surrounding rock. For a nuclear device with the equivalent energy of one kiloton TNT, a sphere of rock 2 m in radius is vaporized, 4 m in radius is melted, and all water in the rock is vaporized out to a radius of approximately 6 m. This interval separates the solid rock from the cavity gases and fluids and defines the initial cavity boundary. The peak acceptance stress of the shock wave at this range is approximately 100 kbars (10 GPa).

With either chemical or nuclear explosives the shock wave is attenuated by energy deposition into the rock and

geometrical attenuation. The geometrical attenuation factor accounts for the divergence of the surface area of the wave front as it propagates. Thus the stress (α) and the peak particle velocity (v) being proportional to the square root of the energy per surface area attenuates at $r^{-\alpha}$ where r is the distance from the source and α = 1 for spherical geometry, 1/2 for cylindrical geometry, and 0 for plane geometry.

Energy deposition into the rock varies as a function of distance from the source. Because the final cavity size is proportional to the square root of the explosive energy in a borehole, it is convenient to use the cavity size as a scale parameter for distance measurements. The shock wave deposits energy into the rock by fracturing, compaction, thermal and kinetic energy. The kinetic energy is then degenerated into the first three by the shear stress in the rock.

Near the cavity wall the rock is pulverized by the shock wave such that even the quartz grains within the rock matrix are crushed. The shock wave fractures the rock in shear deformation out to a distance of approximately 3 (spherical), 12 (cylindrical) cavity radii. The degree of damage (fracturing) decreases exponentially with distance from the source. Beyond the shear fracture region the shock wave displaces the rock such that tensile fractures develop due to the divergence of the displacement, creating a tensile hoop stress. The tensile fracture region extends out to about 5 to 7 cavity radii for spherical events, and to 10 to 24 cavity radii for cylindrical boreholes. These distances will vary due to the depth of burial and the residual strength of the rock. The tensile fractures are usually short isolated fractures that do not increase the permeability.

The initial stages of cavity growth are the result of momentum deposited in the rock by the shock wave. Only in the late stages of cavity growth when the cavity has achieved

full size does the cavity gas pressure begin to dominate the expansion process. Depending on the shear strength, the cavity may either expand past the equilibrium point or slowly to the equilibrium point, equilibrium being determined by the cavity pressure in balance with the external stresses. In spherical geometry, shortly after maximum cavity size has been achieved, the entire region within 2 cavity radii rebounds simultaneously toward the detonation center. This tends to lock in a compressive hoop stress in the media around the cavity and preserve its dimensions.

Chemical and nuclear explosives differ in the magnitude of energy release. Cavities sprung by nuclear explosives are larger than those created by chemical explosives. However, the stress accepted by the medium is similar. The theory described in the next section is justified using both chemical and nuclear explosives and, we believe, works because of the common features displaced by the stress wave when propagating into the rock.

3.0 Explosively Created Permeability

3.1 Previous Theories

Attempts to predict explosive-generated permeability have previously been based on correlating the degree of fracturing or damage caused by the stress wave to the enhanced permeability. The main proponents of these theories were Laspe,[6] Terhune and Shaw,[7] and Butkovich.[8]

Laspe's theory attempts to correlate surface area created from the blast with energy absorption. Laspe assumed that particles in sedimentary rocks are cemented together with a statistical distribution of bonding strengths. A distribution of bond strengths was postulated to give rise to an exponential absorption of energy with distance from the shock analogous to absorption of radiation in a solid.

Laspe suggested that if a material's specific surface energy for fracturing is given, a mean particle diamater as a function of distance can be calculated. Based on mean particle diameter, explosive fracture effects are then divided into a pulverized zone and a fractured and competent zone. Laspe then simplified the treatment of the pulverized zone by assuming it to be similar to a 300 micron (50 mesh) fracture proppant sand. He resorted to a semi-empirical approach for treating the secondary fractured zone. Distribution of permeability is obtained by assuming its decay rate is the same as that for energy, namely exponential. Empirical constants are adjusted to obtain agreement with observation.

A second theory due to Terhune and Shaw is considerably more elaborate than Laspe's. Laspe relied mainly on empirical predictions, which did not use detailed material property data, depth of burial, or explosive source parameters. In contrast, the model of Terhune and Shaw[7] was a detailed mathematical calculation of the non-linear elastic continuum equations describing the response of rock. They also included a fairly complete simulation of the explosive detonation process. Moreover, extensive experimental rock property measurements were used as input to the model. An attempt was made to correlate permeability with failure characteristics of the rock. In particular, they defined a quantity termed "crack number," which referred to the number of times a zone in the calculations exceeded the experimentally measured failure criterion. They found that the "crack number" was a function of zone size. However, they were able to locate a range for which the "crack number" was reasonably insensitive to this quantity.

Terhune and Shaw observed that fluid loss during postshot drillback occurred whenever the "crack number"

exceeded 5. This corresponded to the limit of shear failure on compressive loading and indicated a correlation with enhancement of permeability. They also reported some agreement between inferred permeability distributions from pressure testing and "crack number." However, they concluded that the data were insufficient at that time to attempt to develop a consistent criterion relating crack number to a permeability magnitude.

Another version of the computer model of Terhune and Shaw was used by Butkovich[8] to correlate fracturing effects as well as permeability around detonations. This version, called SOC73, was modified by Schatz.[9] Schatz, instead of computing "crack number" as a measure of fracture damage, used a quantity termed "failure shear strain." Failure shear strain is based on separating the total strain into elastic and "plastic" parts. As the material deforms, the elastic part of the strain is computed from relations based on Hooke's law. If the material fails, the portion of the strain not associated with elastic strain is the failure-associated strain, or "failure shear strain." Failure shear strain is accumulated in a given zone with time and serves as a damage index which can be interpreted in terms of fracture intensity. Butkovich found that the limit of observable fracturing for a cylindrical borehole shot in coal correlated approximately with a value 0.01, for failure shear strain. This corresponded to a distance of 8.5 postshot cavity radii. Butkovich indicated that if the failure shear strain was cubed it displayed the same decay characteristics as the measured permeability distribution.

The above models all have a common approach: They assume that permeability is solely related to the degree of fracturing. High fracture intensity, according to these theories, should result in high permeability. This is not correct and, in fact, can result in lowering permeability.

Permeability depends on both the degree of fracturing and porosity. Attempts to correlate permeability to experimental data for use in predicting permeability without considering porosity must therefore be regarded as theoretically unsound. This is apparent, since none of these approaches can predict the behavior of permeability around an explosive without matching arbitrary parameters to experimental measurements.

A theory that includes both the effects of fractures and porosity was devised by McKee and Hanson.[3,4] Their model appears to be valid for the case in which all fractures are explosively created. This theory was recently extended to include the initial fracture density[5] and is summarized in the following section.

3.2 Theory of Explosively Created Permeability

To obtain an expression for permeability in terms of known parameters in rock mechanics, a constitutive equation is required. The approach of McKee and Hanson[3,5] was to begin with the widely accepted Blake-Kozeny-Carmen theory.[10] For more detail the reader is referred to their papers.

In this theory a wide range of pore geometry[4] results in the expression

$$k = \frac{\phi^3}{CT(1-\phi)^2 S^2} , \qquad (3.1)$$

where C = 3 for fractures, T is the tortuosity, ϕ the porosity, and S the specific surface area.

In the case of explosively created fractures the porosity is much less than one and can be neglected in the denominator. The fracture density (n) can be written in terms of the specific surface area as

$$S = \frac{2nh}{1-\phi} \quad . \tag{3.2}$$

Substituting equation (3.2) into (3.1) and assuming the fractures are pervasive (h = 1), we obtain

$$k = \frac{\phi^3}{4CTn^2} \quad . \tag{3.3}$$

This clearly demonstrates the dependence on both the porosity and the fracture density. Equation (3.3) illustrates the problem with previous theories and their exclusive reliance on attempting to correlate permeability with fracture density. In fact, the above equation indicates that for a given porosity an increase in the number of fractures per unit area will actually decrease permeability. This is due to increased surface area and greater drag on the fluid traveling through the medium.

Hence it is not sufficient simply to create cracks. Porosity must be placed in these cracks. Distribution of a given amount of porosity over a greater number of cracks will reduce the permeability.

To link explosive effects to either of the permeability equations above, we view the explosion as occurring in two stages. The first is dominated by a large-amplitude stress wave, and the second involves an expansion of the cavity by high-pressure gases from the detonation. The effects of the first stage on the medium are of a dynamic nature, while those of the second stage extend over a much longer time interval and can be regarded as a quasi-static process. To obtain a description of permeablity, these processes must be related to the fundamental equations for permeability.

The dynamic stress wave will cause all flaws whose strengths are less than the magnitude of the locally applied stress to extend. A relation between the growth of flaws or the increase in specific surface and energy can be obtained from comminution theory. Several comminution relations have been proposed. The one most applicable to our situation is Rittinger's Law, which states that an increase in specific surface area is directly proportional to the energy input:

$$S \propto E \ . \qquad (3.4)$$

Rittinger's Law has been substantiated by the general scaling laws of Langefors and Kihlstrom,[11] which have been verified for burden dimensions varying between 0.01 and 10 m with a 10^7 variation in explosive charge. Rittinger's Law has been further substantiated by Felts and others[12] in the laboratory, and theoretically by Rose.[13]

Creating fractures does not in itself generate permeability. This is because the stress wave propagates at the compressional-wave velocity (c_p), while fractures can grow in a rectilinear path at a maximum velocity of 1/3 c_p. Hence, the stress wave will inevitably outrun the fractures it generates. New fractures will then be initiated on other flaw sites in the material. At this moment in the process, the medium consists of a noninterconnected system of fractures with essentially no new porosity.

The second stage of the essentially continuous explosion process is dominated by the quasi-static expansion of the gas in the cavity. The cavity void space is produced by irreversible pressure-volume work of the explosive gases. Void space is created by irreversible radial compression and by the tangential tension of the surrounding rock. The fracture porosity will be proportional to the first invariant

of the strain tensor,[14]

$$\phi \propto \Delta \ , \tag{3.5}$$

where Δ is the first invariant and contributes to porosity only when it assumes positive values (dilatation).

Figure 1 shows the postshot configuration. The cavity's initial radius is r_o. The explosion springs the cavity to a larger radius r_c. The material initially between r_o and r_c has been compressed into a narrow region beyond r_c. This material, in trying to recover a fraction of its original size, is locked in. The tangential stress in the locked-in region gives rise to a compressive radial stress or effective pressure.

The power for plane harmonic waves[14] and for cylindrical or spherical waves with dissipation[15] can be expressed in terms of particle velocity or stress squared. We may, therefore, write

$$E \propto \bar{\dot{u}}^2 \propto \bar{T}^2. \tag{3.6}$$

Even for high stress levels, equation (3.6) is still a good approximation. Other criteria will be discussed below. For the case of pervasive fracturing (h = 1) and small porosity, surface area is directly proportional to fracture density, or

$$S \simeq 2n. \tag{3.7}$$

Denoting the explosion-induced fractures by n_e and the naturally occurring ones by n_o, the total specific surface or fracture density becomes

$$n_t = n_o + n_e \ , \qquad (3.8)$$

where

$$n_e = bE \qquad (3.9)$$

and b is a constant of proportionality.

The second or quasi-static stage can be satisfactorily treated by using the bilinear elastic static solutions for dilatation around a pressurized cavity,[3] which can be substituted into equation (3.5) to yield

$$\phi \propto \frac{f - \alpha}{r^{1 + \alpha}} \ , \qquad (3.10)$$

where f = 1 for cylindrical and 2 for spherical symmetries, and

$$\alpha = f - \varepsilon, \qquad (3.11)$$

where ε is a small positive number related to the ratio or elastic constants in compression and tension.[3]

If no bilinearity in the elastic constants is present, then from equations (3.10) and (3.11), dilatation, and hence porosity, would be identically zero. Bilinearity implies the existence of cracks and flaws that are necessary to create permeability. The use of equations (3.10) and (3.11) is supported by displacement measurements reported by Borg.[16]

Combining equations (3.5), (3.8), and (3.9), we obtain the expression

$$k_e \propto \frac{\Delta^3}{(n_o + bE)^2} \qquad (3.12)$$

for the explosively created permeability. The effect of preshot permeability is included by adding to it the explosively generated permeability to obtain

$$k_t = k_e + k_o , \tag{3.13}$$

where k_o is the preshot permeability.

Some limiting cases to equations (3.12) and (3.13) are evident. From equation (3.13), if initial permeability is high, then the explosive's contribution to the total permeability can be negligible. Secondly, if initial fracture density is large compared to that generated by the explosion, then substituting equations (3.10) and (3.11) into (3.12), we obtain

$$k_e \propto 1/r^6 \text{ (cylindrical geometry)} \tag{3.14}$$

$$k_e \propto 1/r^9 \text{ (spherical geometry)} , \tag{3.15}$$

where ε is small compared to f.

Hence, the effect of the explosive decays strongly with distance. On the other hand, if the material is relatively competent or if explosion-induced fractures dominate the initial fracture density, we obtain

$$k_e \propto \frac{\Delta^3}{E^2} . \tag{3.16}$$

From Selberg,[17] energy decays asymptotically in the elastic limit as

$$E \sim 1/r^2 \text{ (dynamic, spherical geometry)} \tag{3.17}$$

$$E \sim 1/r \quad \text{(dynamic, cylindrical geometry)} \tag{3.18}$$

Substituting for dilatation from equation (3.10), we find (for $n_e >> n_o$ and in the elastic limit)

$$k_e \propto 1/r^4 \quad \text{(cylindrical geometry)} \tag{3.19}$$

$$k_e \propto 1/r^5 \quad \text{(spherical geometry)} \; . \tag{3.20}$$

In the general case, energy will obey a power law decay

$$n_e = bE \sim 1/r^{f+m}, \tag{3.21}$$

where f is defined as before (f = 1, 2 for cylindrical and spherical geometry, respectively). In the perfect elastic case, m = 0 (asymptotic limit). However, in general, m is greater than zero. For a competent formation ($n_e >> n_o$), permeability will have the form

$$k \propto \frac{r^{2m}}{r^{3+f}} \; . \tag{3.22}$$

If m = 0, then we recover equations (3.19) and (3.20). Real materials will exhibit dissipation and deviate from elastic behavior (i.e., m will be greater than zero). From equation (3.22) we see that explosion-created permeability can decay much more slowly than for the perfectly elastic case or for the case where the initial fracture pattern dominates. A physical interpretation of this is readily apparent. For the perfectly elastic case, we note that fractures must exist as

continuous rays emanating from the cavity. On the other hand, a real material will exhibit a fracture pattern having a distribution of fracture lengths. For a dissipative material, fracture density decreases more rapidly with distance from the cavity than in the elastic limit. There is always competition between fracture density and porosity. When fracture density decreases with distance from the borehole, as in a real material, surface area declines more rapidly, tending to compensate for the decrease in porosity. Hence, the result is a slower decrease in permeability away from the explosive cavity. This results because an increase in surface area increases drag, and hence resists flow. On the other hand, making porosity larger increases the cross-sectional area to flow, thus decreasing resistance.

4.0 Experimental Results from Single Explosive Detonations

4.1 Hardhat (Spherical Geometry)

The Hardhat event was a 5-kt nuclear explosion in granite. Boardman and Skrove[18] performed extensive air permeability measurements around the Hardhat nuclear chimney. Their raw data show considerable scatter, some of it attributable to their measurement technique. We have applied a selection criterion[3] to their data to obtain a consistent set. As discussed in reference (3), the stress wave decayed approximately as the elastic case. Initial fracture density was taken to be small compared to explosively created fractures. Borg[16] reports that preshot material was broken by fractures, faults, and shear zones, most of which were healed (cemented by minerals of a later origin). She further states that the consensus among geologists is that joints and fractures are short-lived, i.e., terminated within a few yards. The typical flaw size is, therefore, small compared to the cavity radius (20 m) and justifies ignoring the effects of the existing fractures. Figure 2 shows the

comparison between permeability measurements and equation (3.20), the theoretical prediction for an elastic material. Preshot permeability measurements were not performed. However, other initial permeability was estimated to be on the order of tenths to several millidarcies. Agreement between the theoretically predicted slope and the experimental data is quite good. Extrapolating the permeability trend line from the theory yields 65 darcies for k_c, the permeability at $r = r_c$.

4.2 Hoggar (Spherical Geometry)

Delort and Supiot[19] report results of permeability measurements at the French Hoggar test site in the Sahara. Their measurements give a detailed picture of the permeability distribution around the postshot cavities and resulting chimneys.

In view of the fact that explosion-induced fractures are much more numerous than the natural fracture density, we ignore n_o in equation (3.8). Beyond 4 to 5 cavity radii, the explosion-induced fractures will, with increasing distance, blend into the natural fracture system by using equation (3.13). The undisturbed permeability appears to be on the order of 5×10^{-3} μm^2 (5 md).[19]

Explosion-created fracture density can be predicted by combining equations (3.6) and (3.9), to obtain

$$n_e \propto \dot{u}^2. \tag{4.1}$$

Terhune's analysis[20] indicated that particle velocity attenuates with distance as

$$\dot{u} \sim 1/r^{1.6}, \tag{4.2}$$

in agreement with Hoggar measurements.

Equation (4.2) is an asymptotic result, valid for distance greater than 1.5 cavity radii. Nearer the explosive, attenuation is more rapid.

Substituting equation (4.2) into equation (4.1), we find that the fracture density should decay asymptotically as

$$n_e \propto 1/r^{3.2}, \tag{4.3}$$

which corresponds to a value for m of 1.2 from equation (3.13). We recall that $m > 0$ implies greater energy dissipation due to inelastic effects.

Substituting equation (4.3) into equation (3.22), with $f = 2$, $m = 1.2$, yields

$$k_e \propto 1/r^{2.6}. \tag{4.4}$$

Substituting into equation (3.13) with $k_o = 5$ millidarcies (md) and scaling r with respect to the cavity radius, we find

$$k_t = k_c \left(\frac{r_c}{r}\right)^{2.6} + 5 \quad \text{(in md)}, \tag{4.5}$$

where k_c is the intercept at the cavity wall. An approximate fit to the Hoggar data given by Delort and Supiot[19] gives a value of

$$k_c = 1700 \text{ md}. \tag{4.6}$$

The predictions of this theory are in good agreement with the few available observations, as shown in Fig. 3. Data points were taken from reference (19).

4.3 Kemmerer Coal (Cylindrical Geometry)

As part of a coal gasification program, Lawrence Livermore National Laboratory conducted an explosive test in a coal seam near Kemmerer, Wyoming.[21] A cylindrical, high-explosive charge, 5.5 m long, 0.1 m in diameter, and weighing 57 kg, was detonated in a vertical borehole. The center of the explosive charge was located 15 m below the ground surface in a 26-m-thick sub-bituminous coal seam. The postshot cavity radius was estimated from calculations to be 0.17 m. The coal was highly jointed with two joint sets normal to each other. The coal seam was bedded with the bedding dipping at 18°. Mechanical properties as indicated from the logs did not vary appreciably from hole to hole. Permeability tests were conducted in situ from additional holes drilled around the shot hole. Packers were used to insulate sections of the measurement holes and pressure-testing was performed by using water injection until a quasi-steady-state condition was attained. Permeability was then measured at steady state.

Figure 4 shows the results of these measurements with the theoretical prediction equation (3.19) plotted as a straight line. The horizontal lines in the boxes are values of report measurements in the same hole. These represent the uncertainty in the permeability. The width of the boxes along the radial direction is a measure of the uncertainty of the position of the hole at the permeability measurement location. Further details of the experiment are reported elsewhere.[8,21]

Despite a large variation in explosive yield and rock type between the Hardhat nuclear event and the Kemmerer coal experiment, the predictions of theory in both the spherical and the cylindrical symmetries are in agreement with the field measurements. When the rock behaves in a more inelastic manner, an analysis of the decay characteristics of

the dynamic wave is required to provide a prediction of permeability decay away from the explosive cavity. In general, the inelastic characteristic will cause the amplitude of the dynamic wave to decay more rapidly than $1/r$ in the cylindrical case or $1/r^2$ for the spherical geometry. If the material is fairly competent and there is not too much porosity in the existing fracture pattern, then the inelastic behavior will result in the permeability decaying less rapidly than for the elastic case. A least-squares fit to the data[5] indicates that $m = 0.5$ and a permeability decay which is proportional to $1/r^3$. For this case $k_c = 427$ darcies.

5.0 Comparison of Single and Multiple Detonations

The effect of multiple detonations is a straightforward extension of the theory for single charges if certain assumptions are made. These are: (1) that energy fluxes from a number of detonations can be superimposed, (2) that the fracture surface area is directly proportional to cumulative energy input, and (3) that the elastic potential can be superimposed from many cavities to result in a total dilatation which, when positive, is proportional to the porosity increase. The third assumption is not strictly correct unless the bilinear effect is small. The three explosive events discussed above (Hoggar, Hardhat, and Kemmerer coal) tend to substantiate assumption three. We can conclude, therefore, that dilatation, to a close approximation, behaves linearly and that superposition is valid.

The total permeability from a single charge is

$$k = k_c \frac{(\phi/\phi_c)^3}{(n/n_c)^2} + k_o \ , \qquad (5.1)$$

where ϕ is the explosion-created porosity (we are omitting the subscript t on k, the total permeability). Equation (5.1) is derived by substituting equation (3.3) into equation (3.13) and introducing k_c, ϕ_c, and n_o as proportionally and normalizing constants. Rewriting the fracture density to normalize it to n_c, we obtain

$$\frac{n - n_o}{n_c} = r_d^{-f-m} \quad . \tag{5.2}$$

Similarly, from equations (3.10) and (3.11) we obtain

$$\frac{\phi}{\phi_c} = r_d^{-(f+1)} \quad , \tag{5.3}$$

where α has been obtained from equation (3.11) with $\varepsilon << 1$.

Equation (5.1) can also be written in dimensionless form as

$$\frac{k - k_o}{k_c} = \frac{(\phi/\phi_c)^3}{(n/n_c)^2} = \frac{r_d^{-3f-3}}{(r_d^{-f-m} + n_o/n_c)^2} \quad , \tag{5.4}$$

where $r_d = r/r_c$, r_c is the cavity radius.

Figure 5 shows the compared effects of fracture density from equation (5.2), porosity from equation (5.3), and scaled permeability from equation (5.6) for a single explosive charge in different media. Media are not quantified by rock type in a geologic sense, but rather in terms of mathematical parameters such as energy dissipation and initial fracture density required for the theory.

Permeability is the result of substituting the expressions for fracture density and porosity into equation (5.1) for permeability, yielding the formula

$$k = k_c \frac{(r_{1f}^{-2} + r_{2f}^{-2})^3}{(r_{1f}^{-1-m} + r_{2f}^{-1-m} + n_o/n_c)^2} + k_o \ , \qquad (5.5)$$

where the variables are defined in Figure 6 and k_c is the permeability due to a single explosion. The expression is valid when the two explosives have the same strength.

The curves in Figure 7 are obtained by evaluating equation (5.5) along the line of center (x-axis) as done for Figures 7a and 7b.

Permeability again declines sharply due to the fact that porosity enters in the equations for permeability to the third power. We again see the danger of trying to correlate permeability with fracture density alone. Such a correlation would lead one to expect a more gradual decline in permeability with distance, which is incorrect.

All three curves show a slight decrease in permeability as the cavity wall is approached. In Figure 7c, it is only noticeable in the bottom curve. The decrease for the top two curves in Figure 7c is due to the fact that porosity decays more rapidly than fracture density, resulting in a higher contribution to surface area as each hole is approached. The decrease in permeability for the bottom curve is due to increased surface area from the presence of an initial fracture density. The values at $r/r_c = 5$ are doubled over that for a single charge for the top two curves. However, permeability for the bottom curve is enhanced by a factor of 5. This is due primarily to the increased porosity from the second explosive. Enough porosity is added to compensate for initial fracture density.

Of the three cases shown, only the case m = 0 and m = 0.5 is relevant to in-situ mining. The third case is applicable only when the initial fracture density is comparable to that created by the explosion at the cavity wall. The only materials possessing the characteristic would be semiconsolidated sands, which are not good candidates for explosive stimulation.

In a real rock the dissipation factor m will probably range from 0 to slightly greater than 0.5. We will examine the consequences of this in the hydrology section.

6.0 Explosive Selection to Maximize Permeability Enhancement

As can be seen from the previous sections the single most important scaling parameter is the postshot cavity radius or sprung hole diameter. From Figures 5 and 7 it can be seen that permeability enhancement is considerably diminished at a distance of 6-10 r_c from the center of the hole. Accordingly, the larger the postshot cavity radius r_c, the greater will be the distance over which the permeability is enhanced. This leads us naturally into the question of which explosive to use to produce the largest postshot cavity radius r_c, and therefore the maximum extent of permeability enhancement.

Rock blasting and explosives are treated exhaustively in a number of articles and books. Virtualy all the applications are related to the proximity of a free surface. Reflection of the compressional stress from the free surface creates tensional stresses which spall the rock near the free surface and provide relief to enhance breakage. In-situ applications in which the explosive is deeply buried and hence far removed from a free surface have received little attention by comparison.[22]

In formulating a model for explosively expanding the hole from its initial dimensions to a larger diameter we must first understand explosive properties in addition to the rock

properties. Explosives are classified into two categories: ideal and nonideal. Ideal explosives are characterized by a rapid release of energy. The chemical reactions occur on a time scale which is small compared to the time required for gases to expand and the stress wave to propagate into the surrounding rock. Ideal explosives are generally a homogeneous material consisting of one component. TNT, nitromethane, and PETN fall into this category.

Nonideal explosives, on the other hand, require a much longer time to release their energy. Such explosives are multicomponent systems, with fuel and oxidizer usually occurring as fine particulates in physically separated phases.

The detonation velocity for both ideal and nonideal explosives generally lies in the range of 0.5 to 1.0 cm/microsecond. However, the time for total chemical reaction may be on the order of a microsecond for an ideal explosive such as PETN. A nonideal explosive such as ANFO reacts totally in approximately 50-100 μs;[23] the cavity is fully formed in about 3 milliseconds.[22] Their energy content, E_o, is released in a different manner, as illustrated in Figure 8.[24] In Figure 8a (ideal explosive), all the energy is released in the time required for the detonation wave to transverse the explosive. The nonideal explosive releases an initial amount of energy as the detonation wave passes which is significantly less than the total content, as shown in Figure 8-b. This has the effect of slowing the decline of pressure in the cavity so that it can perform more work against the rock and expand the hole to a larger radius. The slower rate of energy release also provides a better impedence match to the rock.[25] It can also result in gas fracturing to appreciable distances from the cavity.[26]

The rapid release of energy from an ideal explosive tends to be manifested in higher frequency components in the stress wave which attenuates rapidly by dissipating its energy in the production of fines. A slower release of energy results in a longer wavelength, greater energy acceptance by the rock, and production of more desirable block sizes.

In enlarging the hole or cavity from its initial dimensions to its final sprung radius, the explosive gases continue to expand until they reach equilibrium with their surroundings. This problem was first studied by Butkovich.[27] He examined the output of extensive computer calculations and compared their productions with observed events from underground nuclear explosions. He found that the gases generated by the explosive expand to an equilibrium state which is determined by the overburden pressure (ρgh) and the strength properties of the medium.[22,27,28] The failure radius, extent of fracturing, and permeability enhancement were found to depend on the final cavity size, in agreement with our results. Several high explosives were compared by Butkovich[22] with different detonation velocities and C-J pressures. He concluded that there was no significant difference in the failure radius due to these quantities: "The main characteristic of the explosive in terms of high explosive fracturing is the value of v/v_o at the final cavity pressure." v/v_o is the volume expansion factor of the explosive, and hence the cavity, over its original specific volume v_o.

The equation describing the adiabatic expansion of an explosive is the JWL expression[29]

$$P_s = Ae^{-R_1 V} + Be^{-R_2 V} + CV^{-(\omega+1)}, \qquad (6.1)$$

where P_s is the pressure under constant entropy or adiabatic conditions, V is the relative value v/v_o, and the remaining constants are parameters appropriate to individual explosives. These parameters are listed in Table 1.[25,30] The qualitative composition of some of the explosives is given in Table 2. Expansion adiabats for the explosives listed in Table 2 are graphed in Figures 9 and 10. The explosives in these figures which perform best are those that produce the largest volumetric expansion in the final cavity pressure range, which is generally below 1 kb (10^8 PA).[5,6]

Examining the effectiveness of the explosives given in Figures 9 and 10 demonstrates that those with an ammonium nitrate base, added oxidizer, and aluminum performed best. These explosives have the highest density and energy content. While military-grade explosives such as TNT and PETN have higher initial pressures at $v/v_o = 1$, they lose their strength to expand the cavity in the critical range in comparison to DuPont's EL-836 and IRECO's DBA-65-T2. Figure 11 depicts the expansion curves in final cavity pressure range. The superiority of these two explosives is even more apparent.

For explosives in boreholes the initial (r_o) and postshot hole radius (r_c) are related by

$$r_c = r_o \left(\frac{v}{v_o}\right)^{1/2} , \qquad (6.2)$$

From the final cavity pressure p_f, the value v/v_o is determined using Figure 12 and substituting into equation (6.2). As previously discussed, the final explosive gas presure at which the cavity stops growing is the sum of overburden pressure and some strength effect of the rock.

Table 1

Equation of State Parameters for Explosives Cited

Name	C-J Parameters					JWL-EOS Coefficients					
	P Mbar	D M/sec	E_0 Mb·cc/cc	ρ g/cc	Γ	A	B	C	R_1	R_2	ω
ANFO	.060	4650	.0325	0.850	2.063	0.4760	.00524	.00720	3.5	.9	.31
POURVEX & POURVEX EXTRA	.130	6100	.0450	1.360	2.893	3.2207	.07769	.00324	4.7	1.4	.16
POURVEX III (EL-836)	.135	5790	.0920	1.520	2.775	2.8123	.02507	.01445	4.5	1.1	.20
DBA-65-T2	.120	5400	.0800	1.520	2.694	2.1467	.02157	.01295	4.3	1.4	.20
UNIGEL	.120	5760	.0510	1.262	2.490	1.9070	.07580	.00627	4.4	1.4	.23
AQUANAL	.055	3700	.0550	1.430	2.559	0.9123	.00407	.00746	4.4	1.0	.16
NITROMETHANE			.051	1.128		2.092	.05689	.0077	4.4	1.2	.30
TOVEX 600	.91	5808		1.572							
TNT	0.210	6930	0.0600	1.630	2.727	3.738	0.03747	0.00734	4.15	0.90	0.35
PETN	0.335	8300	0.1010	1.770	2.640	6.170	0.16926	0.00699	4.40	1.20	0.25

Table 2

Qualitative Comparison of Selected Commercial Blasting Agents[4]

Name	Mfgr	Density gm/cc	Ammonium nitrate	2nd oxidizer	Sensi-tizer	Aluminum	H_2O	Carbonaceous materials
POURVEX III (EL-836)	DuPont	1.52	X	X	X	X	X	X
DBA 65-T2	IRECO	1.52	X	X	X	X	X	X
AQUANAL	Atlas	1.43	X		X	X	X	X
POURVEX	DuPont	1.36	X	X	X		X	X
ANFO	Gulf	.85	X					X
UNIGEL	Hercules	1.28	X	X	X			X

Butkovich did not quantify the strength effect term to enable prediction of p_f from fundamental rock properties. This can be done by constructing a simplified model of the process, which we discuss below.

To obtain the final cavity pressure we assume the cavity growth ceases when the pressure exerted on the cavity wall falls just below the yield strength of the rock. An equilibrium solution for the stresses around a pressurized cavity gives for the stress[14]

$$\sigma_r = p_{ob}\left(1 - \frac{r_c^2}{r^2}\right) + p_c \frac{r_c^2}{r^2} \qquad (6.3)$$

$$\sigma_\theta = p_{ob}\left(1 + \frac{r_c^2}{r^2}\right) - p_c \frac{r_c^2}{r^2} \qquad (6.4)$$

where σ_r = radial stress
σ_θ = tangential stress
p_{ob} = overburden pressure
r_c = cavity radius
r = distance from the center of the cavity
p_c = final cavity pressure.

There are at least seven failure criteria which can be considered.[32] The one most frequently used is that of maximum distortional strain energy, also known as the maximum octahedral shear stress criterion, which is attributed to Von Mises.[14,32] For our use it has the form

$$(\sigma_r - \sigma_\theta)^2 + (\sigma_\theta - \sigma_z)^2 + (\sigma_z - \sigma_r)^2 = 2\sigma_o^2 \qquad (6.5).$$

where σ_o is the yield stress in uniaxial compression.[32] This formula has been used by Scott and others to explain rupture around boreholes.[33] Evaluating the stresses at r = r_c yields

$$\sigma_r = p_c$$

$$\sigma_\theta = 2p_{ob} - p_c. \qquad (6.6)$$

Setting σ_z equal to the overburden pressure p_{ob}, and substituting into equation (6.5) yields

$$p_c = p_{ob} + \frac{\sigma_o}{\sqrt{3}}, \qquad (6.7)$$

where the second term on the right is the shear strength of the rock.[32] The final cavity pressure at which expansion stops is therefore equal to the sum of the overburden pressure plus the shear strength of the rock. This is in general agreement with Bukovich's findings discussed earlier. If the explosive's expansion adiabat is represented by

$$p(v/v_o)^\gamma = c, \qquad (6.8)$$

where γ and c are determined for each explosive from Figure 11, then the cavity radius is given by the espression

$$r_c = \left(\frac{c}{p_{ob} + \frac{\sigma_o}{\sqrt{3}}} \right)^{\frac{1}{2\gamma}} r_o . \qquad (6.9)$$

As an example, let us consider a copper/uranium ore body with an average compressive yield strength of 0.9 kb at a depth of 675 ft. If the overburden density is 1.1 gm/cc, then the overburden pressure is 0.05 kb. Substituting into equation (6.7) results in a final cavity pressure of 0.57 kb. Returning to Figure 11, we can find the volume expansion factor appropriate to each explosive (Table 3).

From Figures 5 and 7 the power law range for permeability decay will limit the spacing of explosives. Depending on k_c (explosively created permeability at the cavity wall), and k_o (initial permeability), the spacing of explosives can probably be no greater than ten to fifteen times the postshot cavity radius apart.

Table 3

Volumetric Expansion Factor for Copper Uranium Ore Body Having Postshot Cavity Pressure of 0.57 kb

Explosive	v/v_o	r_c/r_o
EL-836	15.0	3.9
DBA-65-Tw	13.5	3.7
AQUANAL	9.2	3.0
TOVEX 600	7.8	2.8
ANFO	7.0	2.6
TNT	7.2	2.7
POURVEX	5.0	2.2

Presented with this fact, two alternatives are available. The first is to drill a large-diameter hole, in the range of 24-30 inches, with a drill such as the Ingersoll Superdrill. Or, one might drill a smaller hole approximately 10 inches in diameter and spring the hole to 3.25 feet (39 inches) in diameter using a high-energy explosive such as EL-836, or an equivalent product. This could be followed by reloading with a less expensive ammonium nitrate water-gel type of explosive or ANFO if conditions permit. The follow-up step with ANFO would spring the cavity to 8.5 feet in

diameter (r_c = 4.25 feet). In view of the cost of EL-836 ($1.10/lb)[26] vs. ANFO ($0.10/lb)[26] the second approach may be more cost-effective. These two steps are correctly summarized in Tables 4 and 5, which give hole spacing for each type of explosive. This is based on a final cavity pressure of 0.57 kb from our previous example, and spacings

Table 4.

Hole Spacing for selected explosives vs. hole diameter. Spacing based on 15 times the postshot sprung hole radius (r_c) and cavity pressure of 0.57 kb.

	Diameter			
Explosive	10 in.	24 in.	30 in.	39 in.
EL-836	24 ft.	59 ft.	73 ft.	95 ft.
DBA-65-T2	23 ft.	56 ft.	69 ft.	90 ft.
AQUANAL	19 ft.	45 ft.	56 ft.	73 ft.
TOVEX 600	18 ft.	42 ft.	53 ft.	68 ft.
ANFO	16 ft.	39 ft.	49 ft.	63 ft.
TNT	17 ft.	41 ft.	51 ft.	66 ft.
POURVEX	14 ft.	33 ft.	41 ft.	54 ft.

of $15r_c$ and $10r_c$ as a function of initial hole diameter. Table 4 shows spacings of up to 95 feet using the highest energy explosive, with typical spacings in the range of 40-60 feet. Table 5, based on 10 r_c, is more conservative, with spacings of approximately 40 feet for the higher energy explosives. In each table the explosive bore holes must be loaded over a length which is approximately twice the well spacing, otherwise end effects are important and will reduce the spacing, the amount of reduction to be determined from more detailed calculations.

These calculations for the example problem demonstrate (a) that explosives must be loaded in large-diameter boreholes created either by direct drilling or by initially drilling smaller holes which are sprung and then reloaded; (b) that unless holes are sprung to larger dimensions and reloaded the practical well spacing is limited to between 40 and 60 feet.

Table 5.

Hole Spacing for selected explosives vs. hole diameter. Spacing based on 10 times the postshot sprung hole radius (r_c) and cavity pressure of 0.57 kb.

	Diameter			
Explosive	10 in.	24 in.	30 in.	39 in.
EL-836	16 ft.	39 ft.	49 ft.	63 ft.
DBA-65-T2	15 ft.	37 ft.	46 ft.	60 ft.
AQUANAL	13 ft.	30 ft.	38 ft.	49 ft.
TOVEX 600	12 ft.	28 ft.	35 ft.	46 ft.
ANFO	11 ft.	26 ft.	33 ft.	42 ft.
TNT	11 ft.	27 ft.	34 ft.	44 ft.
POURVEX	19 ft.	22 ft.	28 ft.	36 ft.

7.0 Hydrologic Design Considerations

The equation to calculate the well flow rate, after the formation permeability is enhanced by a single-hole detonation, is[33]

$$\Delta h = \frac{Q}{2\pi T_o}\left[\ln\left|\frac{r_e}{r}\right| + \frac{1}{\alpha}\ln\frac{k_c\left(\frac{r_e}{r_c}\right)^{-\alpha} + k_o}{k_c\left(\frac{r_w}{r_c}\right)^{-\alpha} + k_o}\right] . \quad (7.1)$$

Setting $r = r_o$, in agreement with standard practice, gives the formula for skin enhancement due to the explosive

$$= \frac{Q}{2\pi T_o}\left(\ln\left(\frac{r_e}{r_o}\right) + \text{skin}\right) , \quad (7.2)$$

where r_e is the effective radius, at which Δh tends to zero, and is given by

$$r_e^2 = \frac{2.25\ T_o t}{S_o} , \qquad (7.3)$$

where T_o and S_o are the undisturbed transmissivity and storage coefficient. The skin factor indicates the degree of improvement in the well flow rate due to the explosive.

Let us now consider the case shown in Figure 12 and use it as a model ore body to illustrate the hydrologic concepts involved in explosive permeability enhancement. Its permeability is taken as 3 md based on the correlation given in Figure 13.[34] Other ore body characteristics are

Depth to top of ore body	600 ft.
Ore body thickness	150 ft.
Depth to water table	300 ft.
Ore body storage coefficient	10^{-5}
Preshot borehole diameter	1 ft.
Postshot cavity radius (r_c)	3 ft.
Well spacing	10 r_c and 15$_c$

For each postshot hole, permeability has the form

$$k = k_c \left(\frac{r}{r_c}\right)^{-\alpha} + k_o \quad . \qquad (7.4)$$

with $\alpha = 4$, for elastic behavior, and $\alpha = 3$ to include the dissipation characteristics of real explosives.

In the case of two-well explosive detonations, there is one injection well and one production well separated by a distance of r. The fluid is circulated between the two wells. Applying the methods of superposition as an approximation, we can use previous equations to estimate the flow rate

$$\Delta h = \frac{Q}{2\pi T_o}\left[\ln\left(\frac{r}{r_o}\right) + \text{skin} - \frac{1}{\alpha}\left(\frac{k_c\left(\frac{r_e}{r_c}\right)^{-\alpha} + k_o}{k_c\left(\frac{r}{r_c}\right)^{-\alpha} + k_o}\right)\right] \quad (7.5)$$

Using the same assumptions, we have estimated the flow rates for the cases of $r = 10\ r_c$ and $15\ r_c$.

The results of the calculations for simple and two-well detonations are given in Figures 14 and 15. The injectivity in gallons/minute is plotted as a function of the permeability enhancement factor k_c/k_o. Pumping rates for the single explosively stimulated well are in the range of several gallons/minute as compared to a preshot rate of 1.5 gpm. With two wells working as an injection-production pair, the flow rate is considerably more than doubled. This is because the second well's enhanced permeability overlaps that of the first well and provides a pressure relief. This illustrates the importance of proper interpretation if the test uses only one explosive and the desirability of an additional shothole to obtain a better idea of the potential flow rates. To obtain an idea of the flow rates we refer to Table 6.

Table 6

Permeability Enhancement Factor

Site	Rock type	Explosive	k_o	k_c	k_o/k_c
Hardhat	Granodiorite	Nuclear	.001 d	65 d	65000
Hoggar	Granite	Nuclear	.005 d	1.7 d	340
Kemmerer	Coal	Chemical	1 d	427 d	427

While the data in the table relies on nuclear explosives, we recall from section 2 that the acceptance stress into the rock is comparable with chemical explosives. Permeability enhancement effects should therefore bear some similarities.

If these assumptions are acceptable, while recognizing the limitations of the data one could expect ratios of k_c/k_o in the range of 300 to several thousand. This implies that for the model ore body flow rates should be enhanced from ten gpm up to as much as 100 gpm. These rates are similar to those occurring in conventional permeable ore bodies in Texas and Wyoming and lend encouragement to the feasibility of in-situ mining of hard-rock ore bodies.

8.0 In-Situ Mining Applications

A complex, deep-seated copper/uranium ore deposit will illustrate one in-situ scheme for metal recovery after blasting. Core samples from this deposit revealed the following characteristics:

1. Depth to ore	300 m
2. Ultimate compressive strength plus overburden stress	1.0 kb
3. Copper content	1-3% Cu
4. Uranium content	0.02-0.06% U_3O_8
5. Major minerals	Quartz, Magnatite, Hematite, Pyrite, Chalcopyrite, Feldspar, Mica
6. Minor minerals	Sphalerite, Bannerite, Gold, rare earths
7. Pyrite/Chalcopyrite ratio	Approx. 1.0
8. Fe/Cu ratio from sulfide minerals	Approx. 1.0

For this depth the cavity size would be only slightly reduced over that shown in the previous section.

8.1 Hydrometallurgy

Samples were ground to -200 mesh for preliminary auto-

clave leach tests. The lixiviant[36,37] was water, adjusted to an initial pH of 2.0 with sulfuric acid, and a high concentration of dissolved oxygen. Final pH after leaching tests varied from 3 to 4. Final condition of ground samples showed almost complete conversion to fine particles of hematite and quartz. Results of four sample leach tests are shown in Table 7.

Table 7

Leach Test Results

Test no.	Temp (°C)	Agitation rate (rpm)	Oxygen press. (psi)	Leach time (days)	Copper recovery (% Cu)	Uranium recovery (% U_3O_8)
1	70	1000	800	5	56	99
2	90	400	500	19	69	70
3	90	400	1000	7	91	88
4	90	None	1000	2	--	--

Test #4 was a leach test primarily on the host rock material to determine the rate of disintegration. Five sample cubes of 1 cm on a side were used. After one day almost total disintegration of the cubes was observed, and the product was primarily fine and coarse hematite and quartz particles.

The results of these and other tests indicate that in-situ solution mining of this particular ore using oxygen at high pressure can potentially leach at an economical rate, and that the host rock would disintegrate at a rate fast enough to keep pace with sulfide leaching.

8.2 Well Completion

As mentioned previously, we assumed that fairly large diameter blastholes could be drilled to moderate depths, economically, using air percussion techniques as exemplified by the Ingersoll Rand Superdrill.

One possible technique is presented to complete injection and production well that should be relatively inexpensive. After detonation the blast holes above the mineralized zone are shown in Figure 16 to be cased with either PVC or fiberglass pipe (6-12" diameter). This outer casing would be secured in place with acid-resistant concrete.

Inside the injection well casing are shown two pipes. The inner pipe is a retrievable perforated s.s. downhole injector pipe. Around it is shown a fiberglass pipe for protection of the s.s. injector. The inner two pipes are set in place as deep as possible below the overburden using high-pressure water jetting, followed by insertion of the injector pipe. In actual practice, injection and production wells should be interchangeable to reverse flow of lixiviant for better utilization of oxygen, thereby increasing overall metal recovery.

8.3 Wellfield Pumping Facility

Figure 17 shows a high-pressure circulation pump moving the lixiviant through the induced-fractured ore zone. This high-pressure circulation loop is developed in line with a filtration unit; such a filtration system is important to any in-situ project since considerable solid waste (i.e., sand and hematite) will be recovered during in-situ leaching and should be disposed of, continuously, with a minimum loss of dissolved oxygen.

8.4 Metallurgical Facility

Figure 18 shows a bleed stream being diverted to a metallurgical plant when metal values reach a desired level. This bleed stream is simultaneously replaced with barren lixiviant from wellfield surge.

Figure 18 is a simplified flow diagram for the recovery of both uranium and copper. Uranium is recovered by ion exchange using an acid elution scheme followed by peroxide precipitation. The uranium peroxide slurry is pumped to a vacuum dryer. The copper is recovered by the more commonly used solvent extraction method. Any organic reagent loss returned to the wellfield system will be oxidized in situ.

If gold and/or silver are present in this type of ore, their recovery is now possible using any one of several lixiviants developed by In-Situ, Inc., that are environmentally acceptable. The low-pH lixiviant used for leaching copper and uranium is first transferred to a new pattern, and water with the new gold or silver leach reagent is added. No oxygen is needed in this new leach circuit. Gold or silver are recovered using a new ion exchange process. Resin elution is fast and complete in less than 10 bed volumes, and the pregnant eluate is ideally suited for direct electrolytic recovery.

In summary, the practical aspects of in-situ mining are presented whereby blasting induces the initial permeability necessary for startup of a leach circult. A powerful, inexpensive lixiviant is shown to be capable of leaching the metal sulfides, thereby increasing the fractured permeability of the host rock matrix. Feasible methods for drilling, well completion, leaching, and metal recovery are discussed to demonstrate one approach to develop the in-situ mine.

References

1. Wadsworth, M. E., "Interfacing Technologies in Solution Mining," Mining Engineering, Dec. 1977, pp. 30-33.

2. Hanson, M. E., R. W. Terhune, and C. R. McKee, "Explosion Phenomenology and Permeability Enhancement in Earth Media," Proceedings, 1981 Explosives Conference of the Internation Association of Drilling Contractors, June 9-11. International Association of Drilling Contractors, P.O. Box 4287, Houston TX 77210.

3. McKee, C. R., and M. E. Hanson, "Explosively Created Permeability from Single Charges," Soc. Pet. Eng. J. 15:495 (1975).

4. McKee, C. R., M. E. Hanson, and R. W. Terhune, "Permeability from Single and Multiple Detonations of Explosive Charges," World Mining and Methods Technology, A. Weiss, ed., AIME, v. 1, p. 365 (1972).

5. McKee, C. R., M. E. Hanson, and R. W. Terhune, "Permeability from Single and Multiple Detonations in Boreholes," In-Situ 1(1):37-73 (1977).

6. Laspe, C., "How to Predict Explosive Stimulation Results," Petr. Engr., May 1971, p. 68.

7. Terhune, R., and J. Shaw, Calculation of Rock Fracturing from Multiple Nuclear Explosive Sources, Rept. UCRL-74017, Lawrence Livermore Laboratory, Livermore, CA (1972).

8. Butkovich, T., "Correlations between Measurements and Calculations of High-Explosive-Induced Fractures in a Coal Outcrop," Int. J. Rock. Mech. Min. Sci. 13:45-51 (1976).

9. Schatz, J., SOC73, A One-Dimensional Wave Propagation Code for Rock Media, Rept. UCRL-51689, Lawrence Livermore Laboratory, Livermore, CA (1974).

10. Carmen, P., "Fluid Flow through Granular Beds," Trans. Inst. Chem. Engrs., London, 15:150 (1937).

11. Langefors, U., and B. Kihlstrom, The Modern Technique of Rock Blasting, John Wiley & Sons, New York (1967).

12. Felts, L., G. Clark, and J. Yanick, "A Laboratory Method of Determining the Thermodynamic Efficiency of High Explosives," Trans. AIME, March 1956, p. 318.

13. Rose, H. E., "A Comprehensive Theory of the Comminution Process," Proc. 2nd European Symposium on Size Reduction (1966), Verlag Chemie, Amsterdam, Decima-Monograph No. 993-1026 (1967).

14. Jaeger, C., and N. G. W. Cook, Fundamentals of Rock Mechanics, 3d ed., Chapman & Hall, London (1979).

15. Hanson, M., and C. McKee, SAFE (Synergetic Acoustic Fracturing Effect), Rept. UCRL-51822, Lawrence Livermore Laboratory, Livermore, CA (1975).

16. Borg, I. Y., Some Shock Effects in Granodiorite to 270 Kilobars at the Piledriver Site, v. 16 Geophysical Monograph Series, AGU, Washington, D.C. (1972).

17. Selberg, H. L., "Transient Compression Waves from Spherical and Cylindrical Cavities," Arkiv for Fysik 5:97 (1952).

18. Boardman, C. R., and J. Skrove, "Distribution in Fracture Permeability of a Granite Rock Mass Following a Contained Nuclear Explosion," Trans AIME 237:619 (1966).

19. Delort, F., and F. Supiot, "Nuclear Stimulation of Oil Reservoirs," Proc. Symposium on Engineering with Nuclear Explosives, Conf. 700101, v.1, p. 649. Amer. Nuc. Soc., Hinsdale, IL (1970).

20. Terhune, R. W., Comparison of Computer Model Predictions of Nuclear Explosion Effects in Hoggar Granite with Experimental Measurements, Rept. UCRL-74306, Lawrence Livermore Laboratory, Livermore, CA (1972).

21. Hearst, J. R., Fractures Induced by a Contained Explsion in Kemmerer Coal, Rept. UCRL-57790, Lawrence Livermore Laboratory, Livermore, CA (1975).

22. Butkovich, T. R., Some Studies of Deeply Buried High Explosive Rock Fracturing, Rept. UCRL-16526, Lawrence Livermore Laboratory, Livermore, CA (1974).

23. Cook, M. A., The Science of Industrial Explosives. Ireco Chemicals, Salt Lake City, UT (1974).

24. Larson, D. B., G. D. Anderson, T. R. Butkovich, and J. R. Hearst, In-Situ Coal Gasification, Progress on the Experimental and Calculational Coal Fracture Program, July-November 1975, Rept. UCID-16651, Lawrence Livermore Laboratory, Livermore, CA (1975).

25. Finger, M., E. Lee, F. H. Helm, R. Boat, H. Cheung, J. Walton, B. Hayes, and L. Penn, "Characterization of Commercial, Composite Explosives," 6th Detonation Symposium, pp. 729-739, Office of Naval Research Report No. ACR-221 (1976).

26. Coursen, D. L., DuPont Research, Potomac River Laboratory, Martensburg, WV, private communication (November 1981).

27. Butkovich, T. R., Use of High Explosives for Springing Underground Cavities, Rept. UCID-15145, Lawrence Livermore Laboratory, Livermore, CA (1967).

28. Butkovich, T. R., The Gas Equation of State for Natural Materials, Rept. UCRL-14729, Lawrence Livermore Laboratory, Livermore, CA (1967).

29. Lee, E. L., and H. C. Hornig, Adiabatic Expansion of High Explosive Detonation Products, Rept. UCRL-50422, Lawrence Livermore Laboratory, Livermore, CA (1968).

30. Finger, M., E. L. Lee, F. H. Helm, B. Hayes, H. Hornig, R. McGuire, and M. Kahara, "The Effect of Elemental Composition on the Detonation Behavior of Explosives," 6th Detonation Symposium, pp. 710-722, Office of Naval Research Report No. ACR-221 (1976).

31. Michaud, L., Explosions nuclaires souterraines des rayons de carite, Rept. CEA-R-3594, Commissariat a l'Energie Atomic (1968).

32. Jaeger, J. C., Elasticity, Fracture, and Flow, John Wiley & Sons, New York (1956).

33. Scott, P. P., W. G. Bearden, and G. C. Howard, "Roof Rupture as Affected by Fluid Properties," Trans AIME 198:111-124 (1953).

34. McKee, C. R., and S. C. Way, "Pressure response equations for explosively stimulated wells," to be published 1982.

35. McKee, C. R., "Permeability of Hard Rock Ore Deposits," to be published 1982.

36. Pitt, C. H., and M. E. Wadsworth, An Assessment of Energy Requirements in Proven and New Copper Processes, DOE/CE/40132, NTIS, Springfield, VA (1980).

37. U.S. Energy Research & Development Administration, Kennecott Copper Corp., and Lawrence Livermore Laboratory, In Situ Leaching of a Nuclear Rubblized Copper Ore Body, vols. I and II, Rept. NVO-155, U.S. Energy Research & Development Administration (1975).

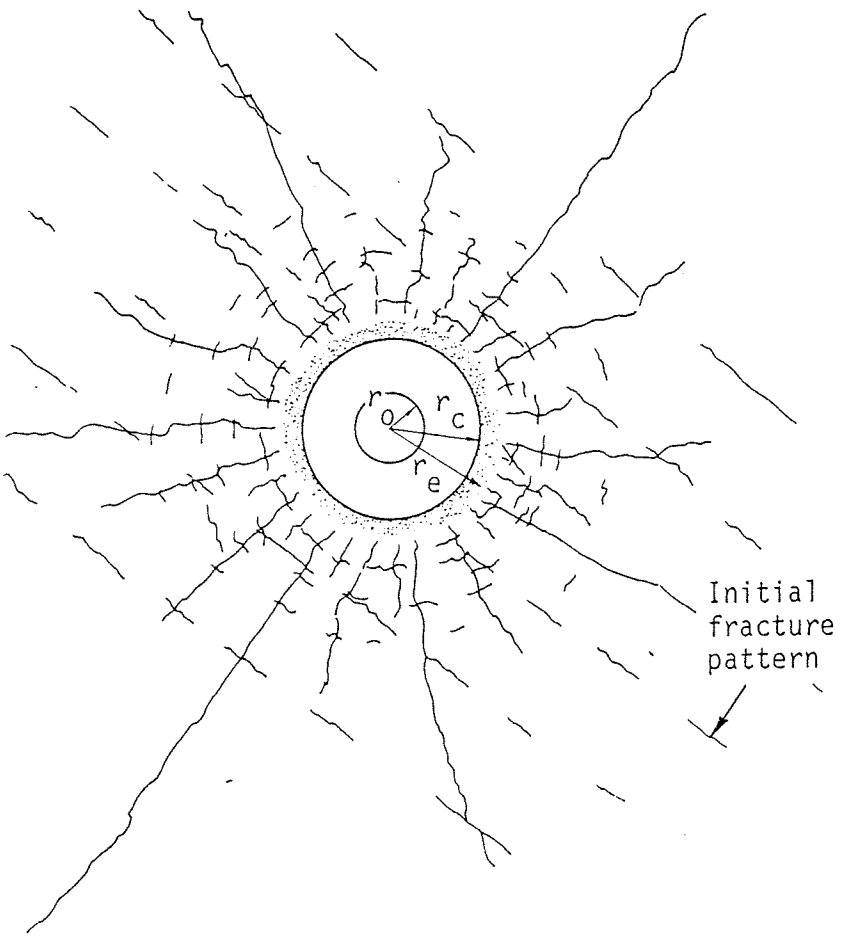

Figure 1. An illustration of the postshot configuration for an explosive fired in a borehole. The sketch includes an initial fracture pattern with the explosive patterns. The preshot radius is r_o, the postshot radius is r_c, and the limit of significant compaction is r_e.

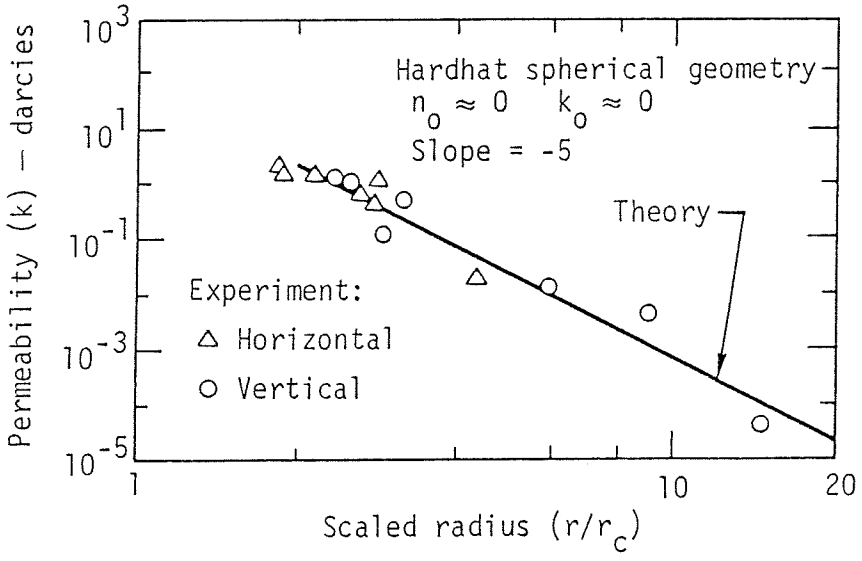

Figure 2. Comparison of theoretical and measured permeability, k, as a function of distance scaled in terms of the cavity radius r_c. Permeability was measured in both horizontal and vertical holes and is independent of direction. The experiment was Hardhat, a 5-kt nuclear explosion in granite at the Nevada Test Site.

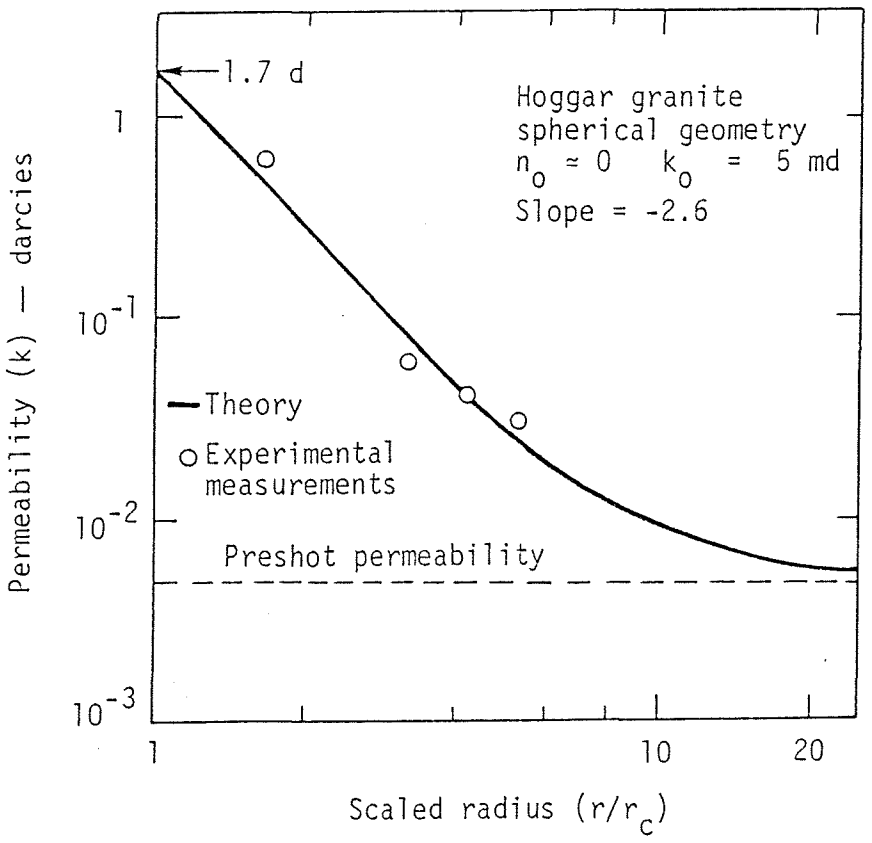

FIgure 3. Comparison of theoretical and measured permeability values. The log of permeability, k, is given as a function of distance scaled in terms of cavity radius r_c. The data are taken from a series of nuclear detonations in the Sahara by the French.

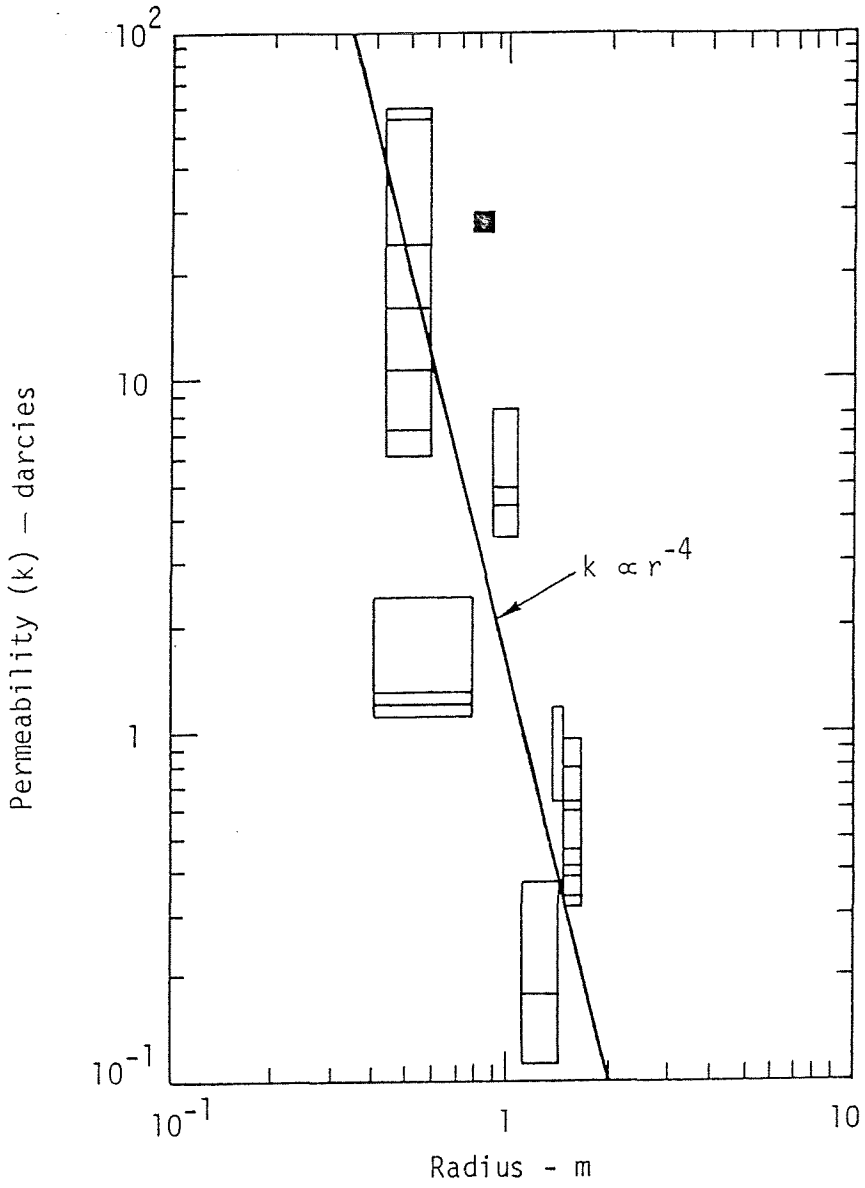

Figure 4. Postshot permeability vs radius for a chemical explosive detonated in a coal seam. The emplacement geometry possessed cylindrical symmetry. Permeability is in darcies, while the radial distance in meters is measured from the axis of symmetry. The small box on the upper right represents two measurements in the same borehole.

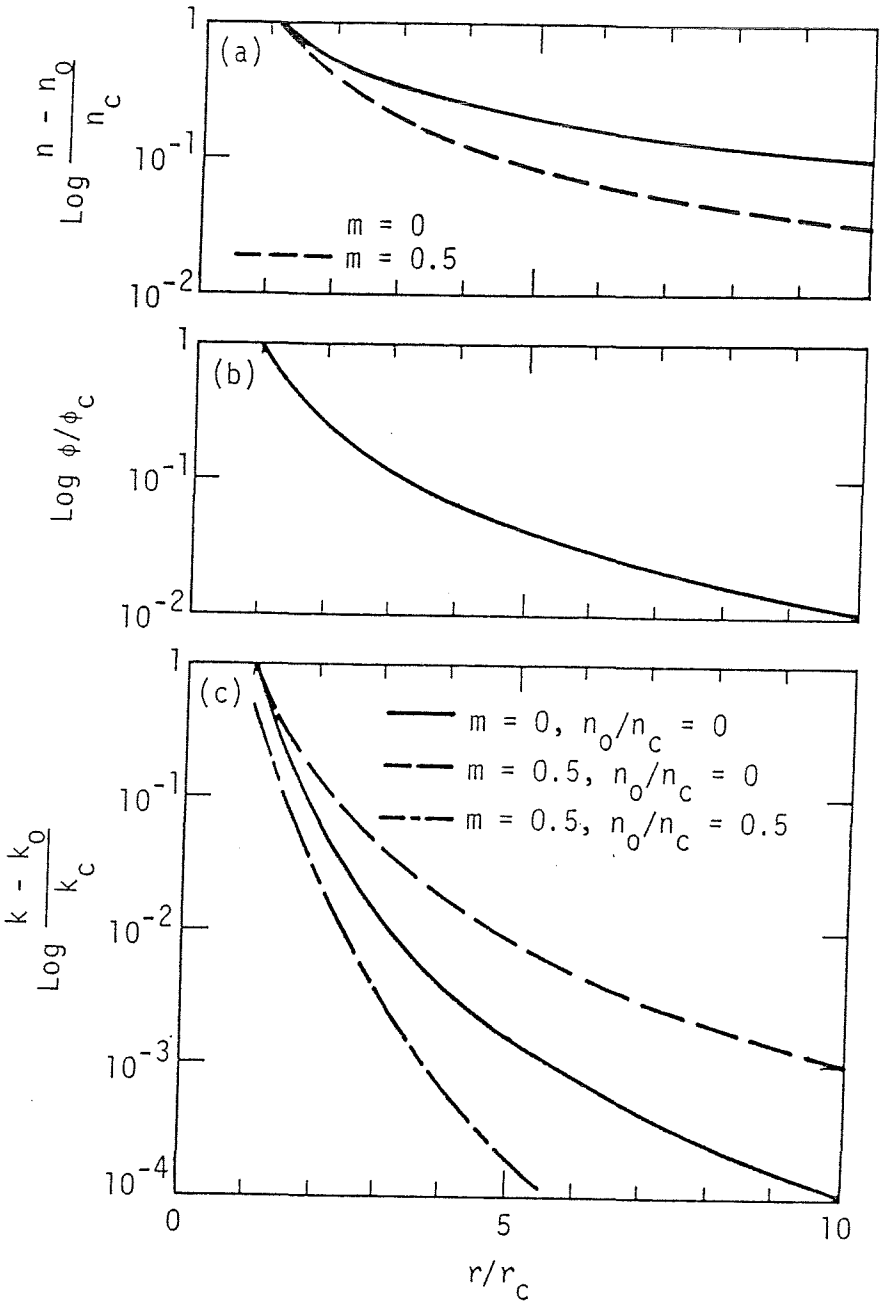

Figure 5. (a) Explosion-induced fracture-density enhancement, normalized to the fracture density at the cavity wall as a function of scaled distance. The solid curve represents a semielastic medium (m=0) and the dashed line a dissipative medium (m=0.5). (b) Explosion-induced porosity, normalized to porosity at the cavity wall as a function of scaled distance. (c) Explosion-induced permeability enhancement, normalized to the permeability at the cavity wall. Three cases are shown: (1) a semielastic medium with zero initial fracture density, (2) a dissipative medium (m=0.5) with zero initial fracture, and (3) a dissipative medium with an initial fracture density of half the explosion-induced fracture density at the cavity wall (m=0.5)

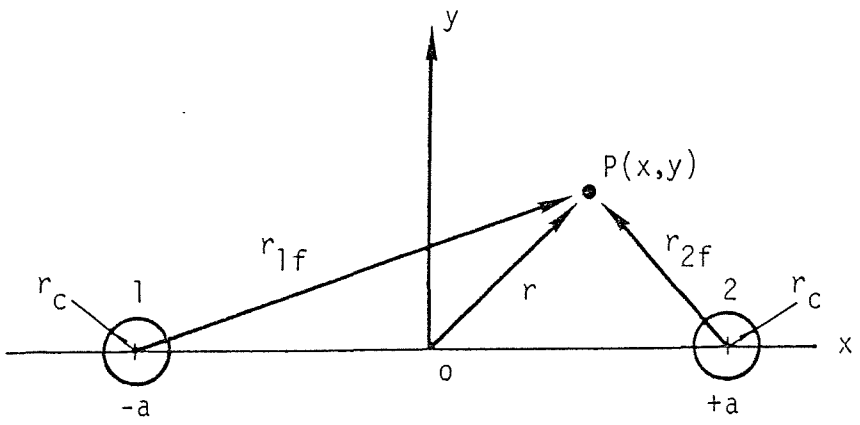

Figure 6. Schematic illustrating the coordinate system for superposition of single charge effects to simulate multiple detonations.

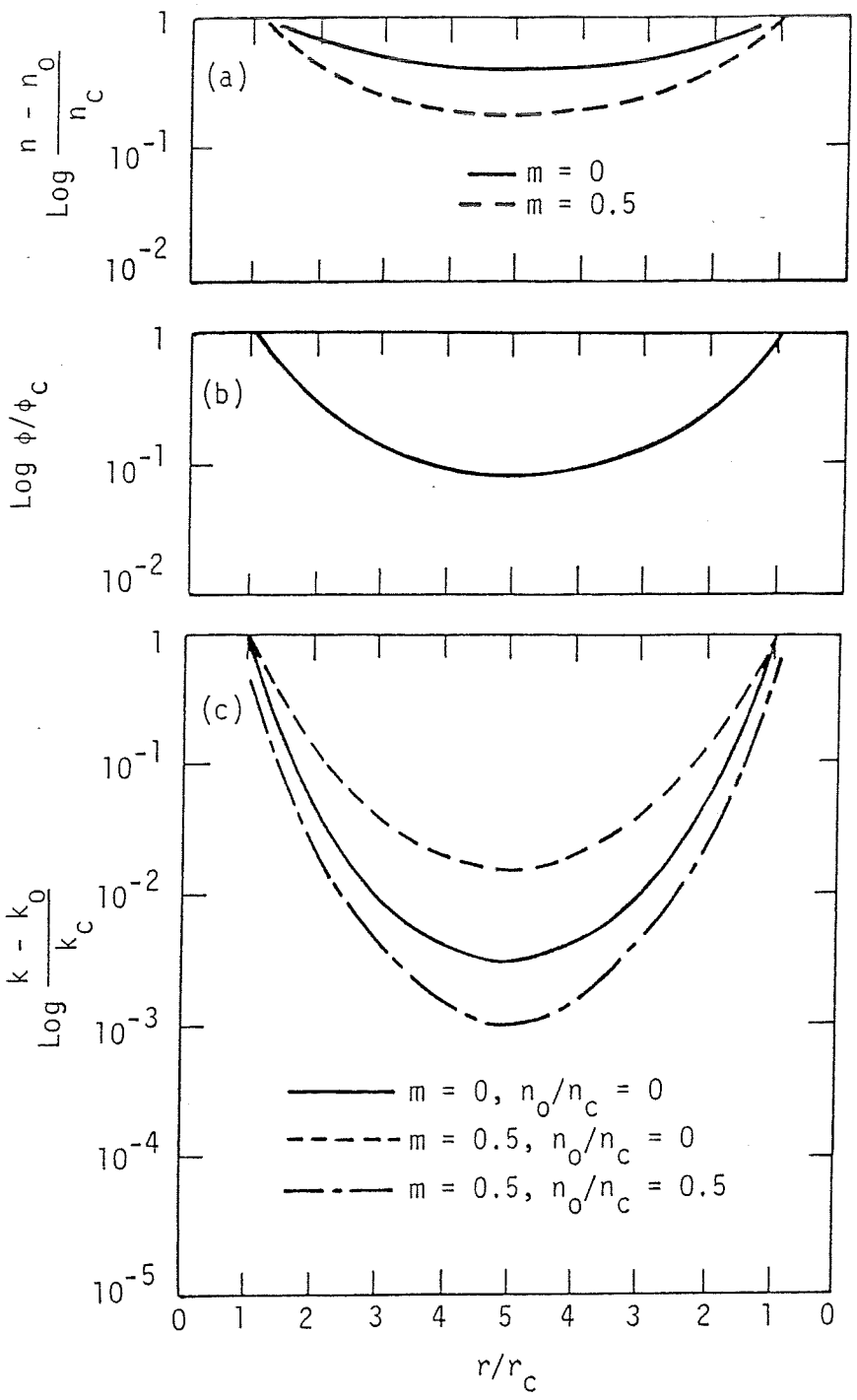

Figure 7. Parameter study for multiple detonations showing variations along the x-axis in terms of scaled distance. r_c is the cavity radius of a single charge. (a) Explosion-induced fracture-density enhancement between two cylindrical charges, normalized to the fracture density at the cavity wall of a single charge. The upper curve is for a semielastic medium (m=0) and the lower for a dissipative medium (m=0.5). (b) Explosion-induced porosity normalized to the induced porosity at the cavity wall between two cylindrical charges at 10 r_c spacing. (c) Explosion-induced permeability enhancement between two cylindrical charges.

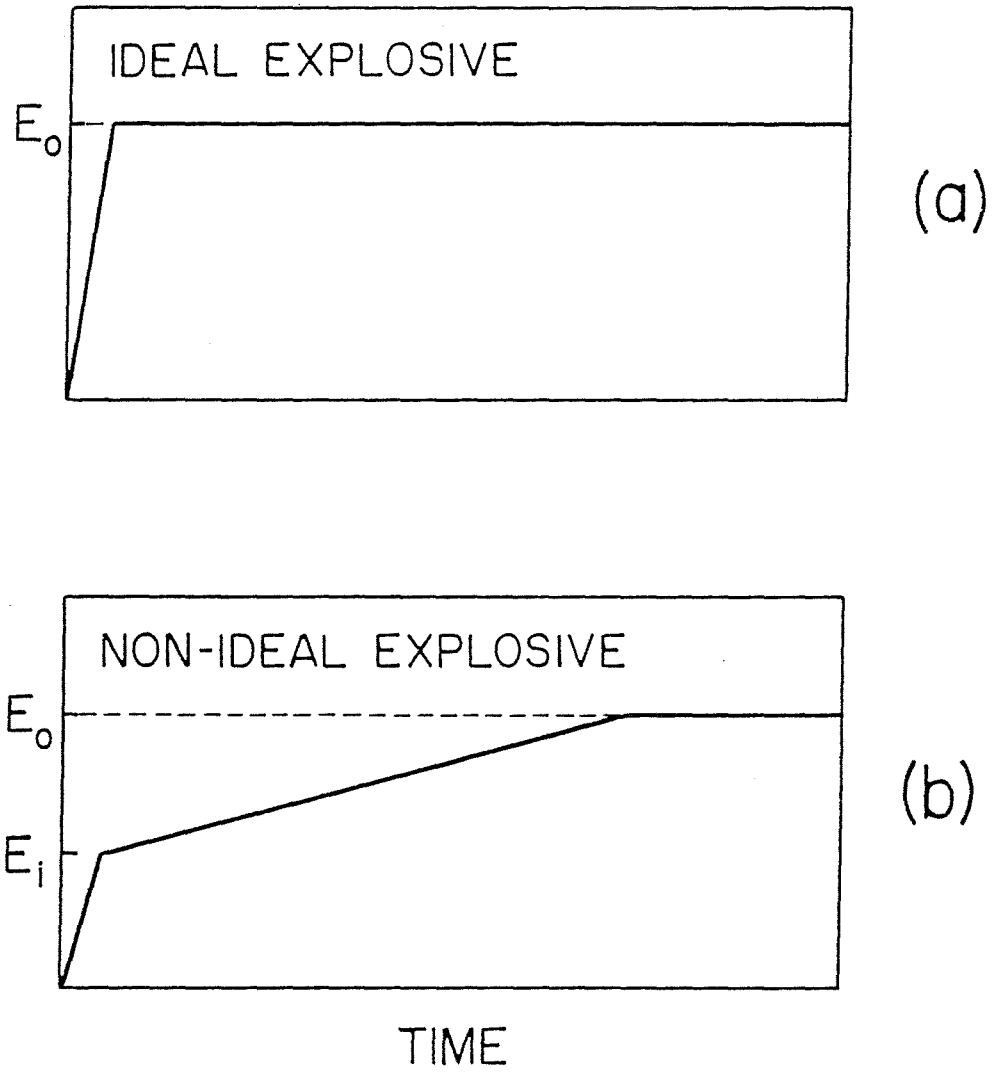

Figure 8. Energy release rate for ideal(a) and non-ideal (b) explosives.

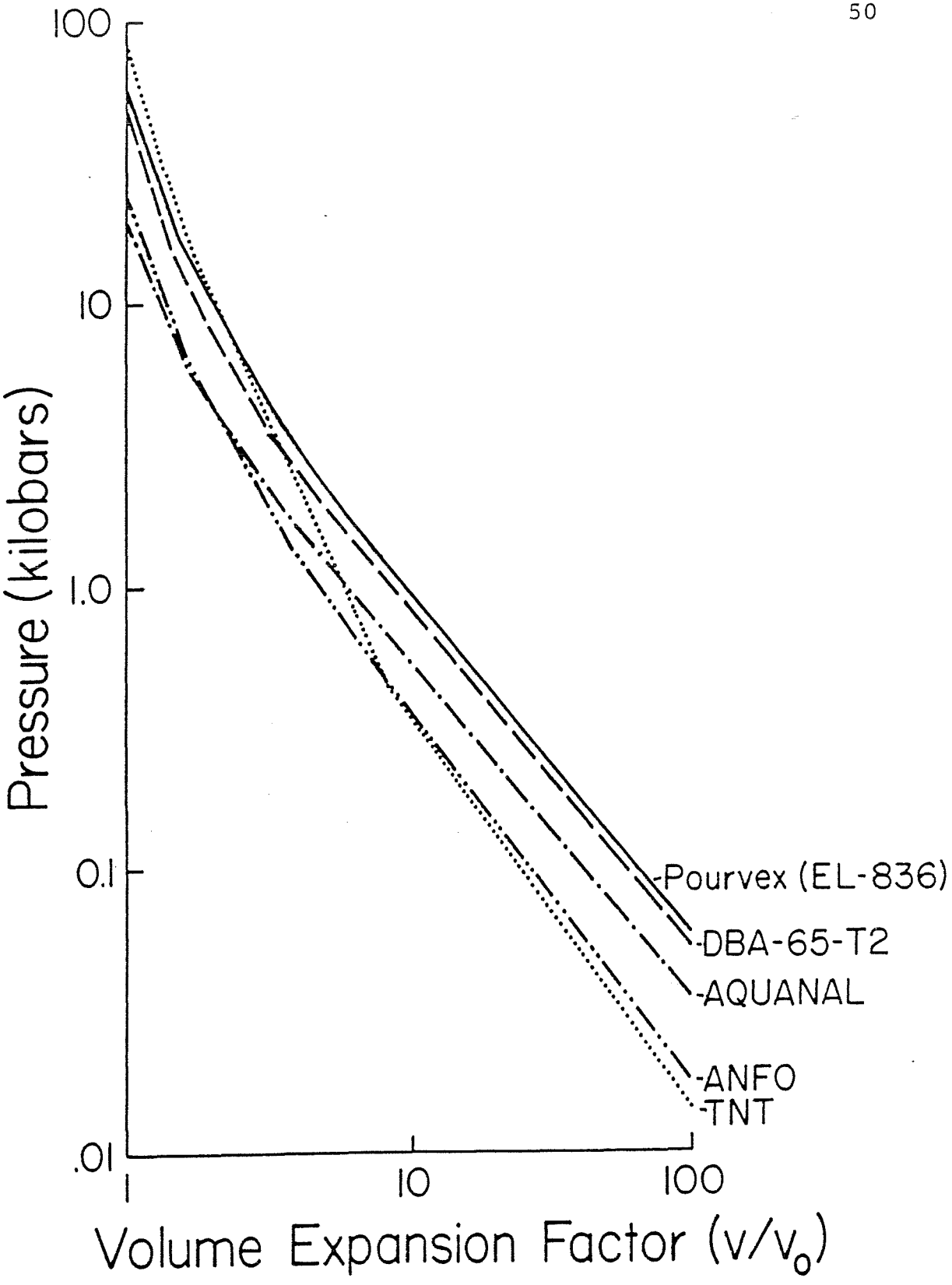

Figure 9. Explosive expansion adiabats.

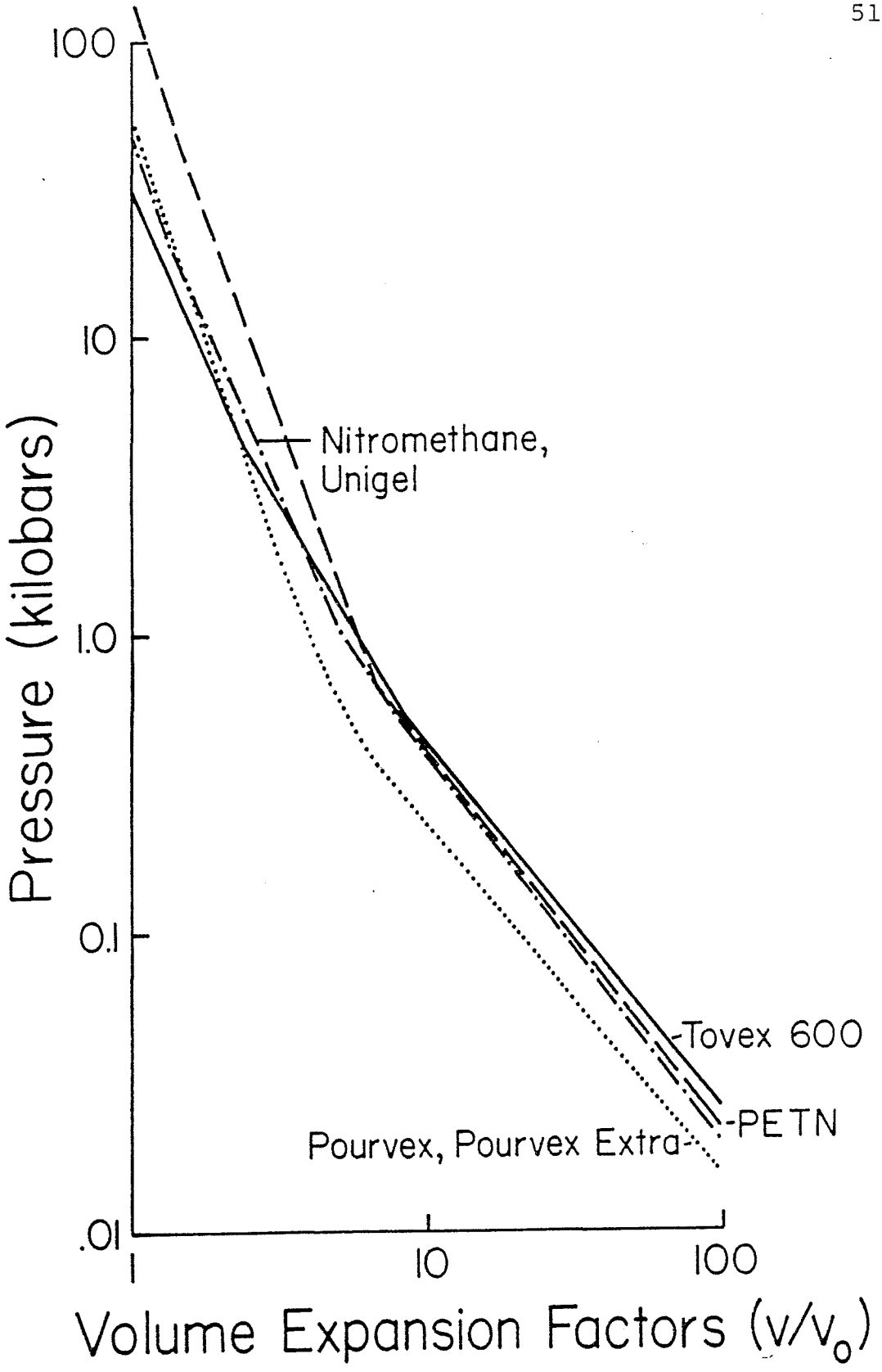

Figure 10. Explosive expansion adiabats.

Explosive Expansion Curves
Final Cavity Pressure Range

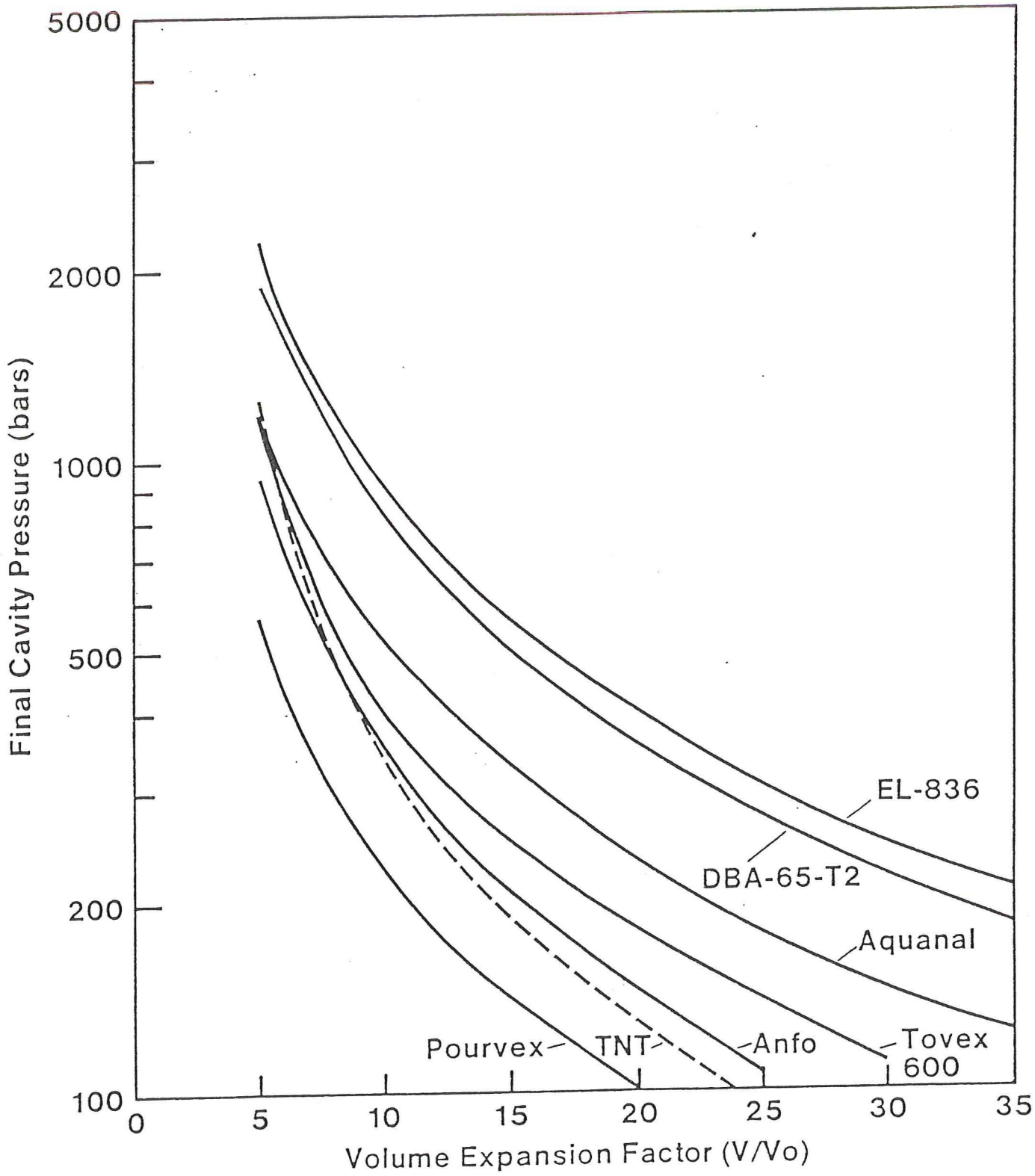

Figure 11.

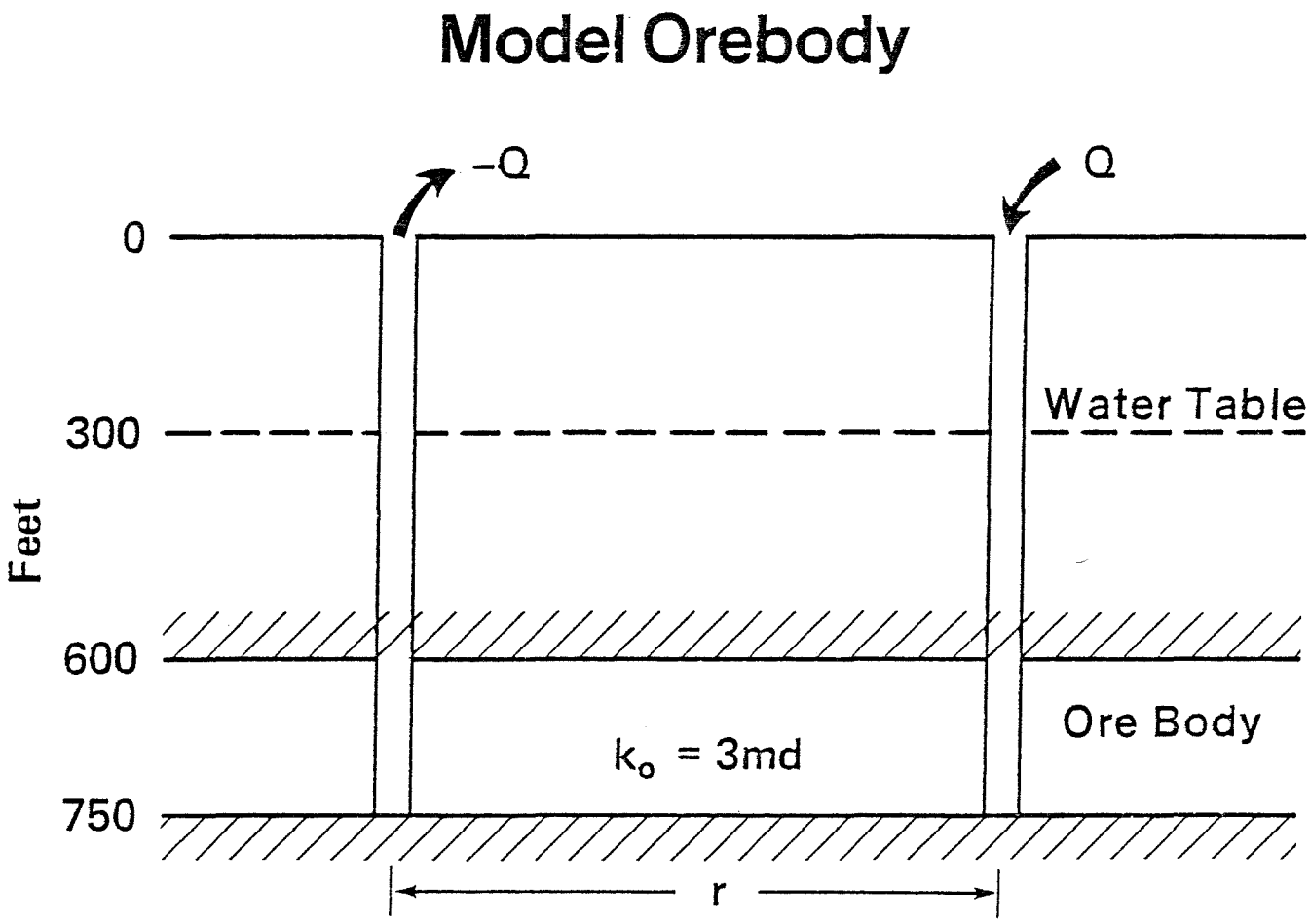

Figure 12. A model ore body used to illustrate the hydrologic concepts involved in explosive permeability enhancement. The effects of stimulating one well and then two wells are examined as to their injectivity and productivity.

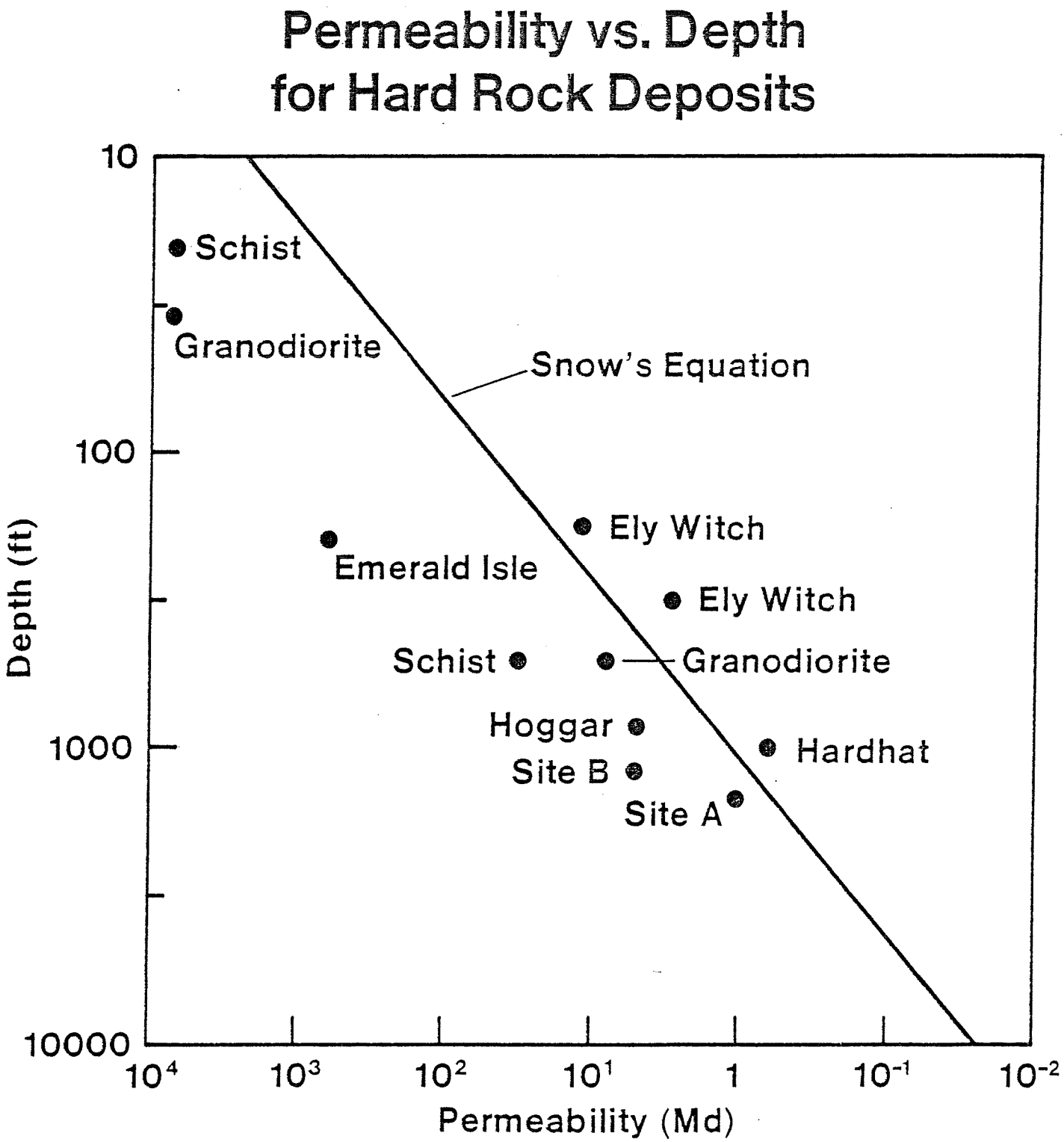

Figure 13. Permeability vs. depth for hard rock ore deposits. Most formations and ore bodies studied follow Snow's trend line but with generally higher permeability for a given depth. At depths of 1000 ft permeabilities in the range of 1-10 md may be expected.

Injectivity-Productivity for Model Orebody vs. Explosive Permeability Enhancement

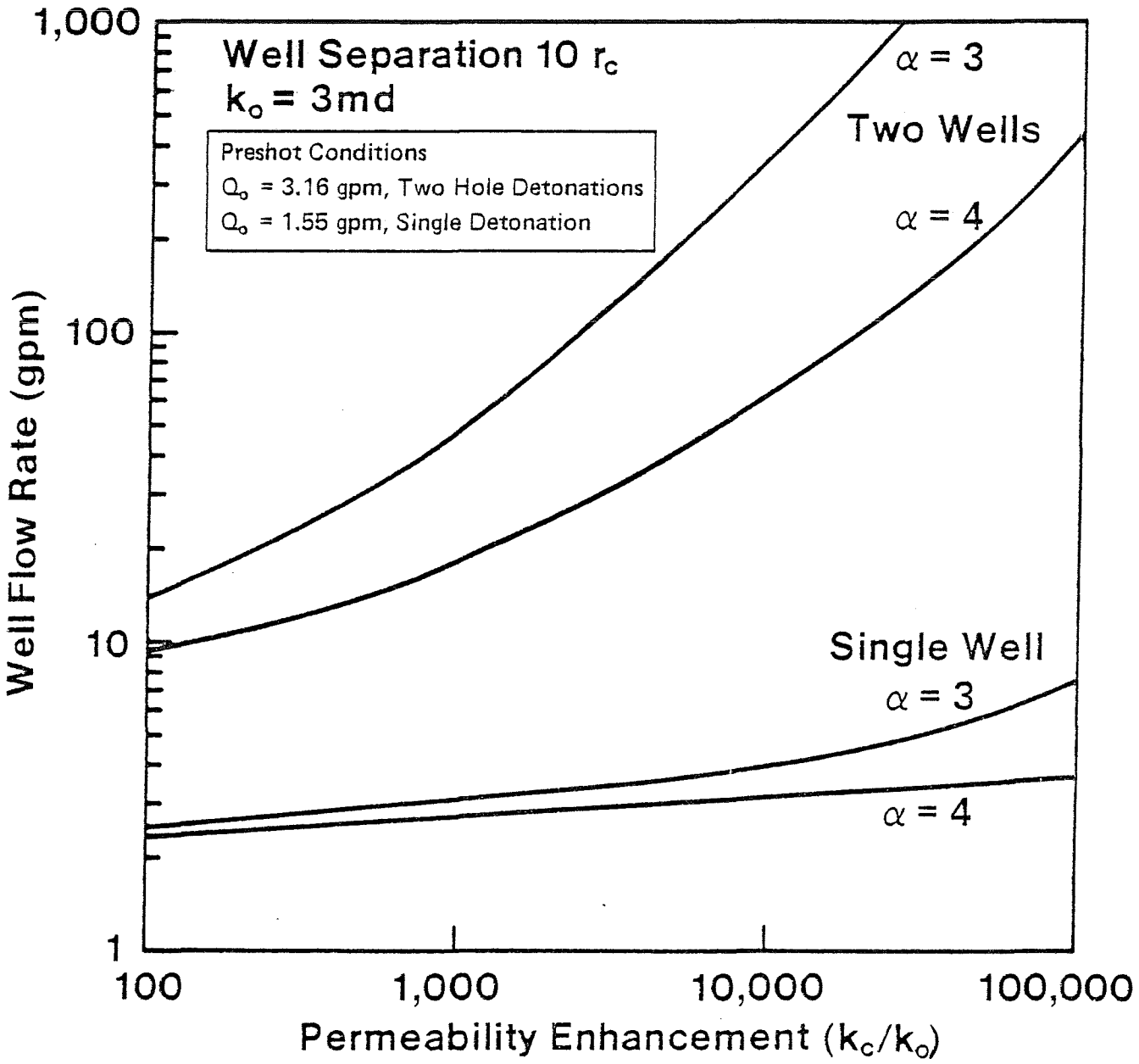

Figure 14.

Injectivity-Productivity for Model Orebody vs. Explosive Permeability Enhancement

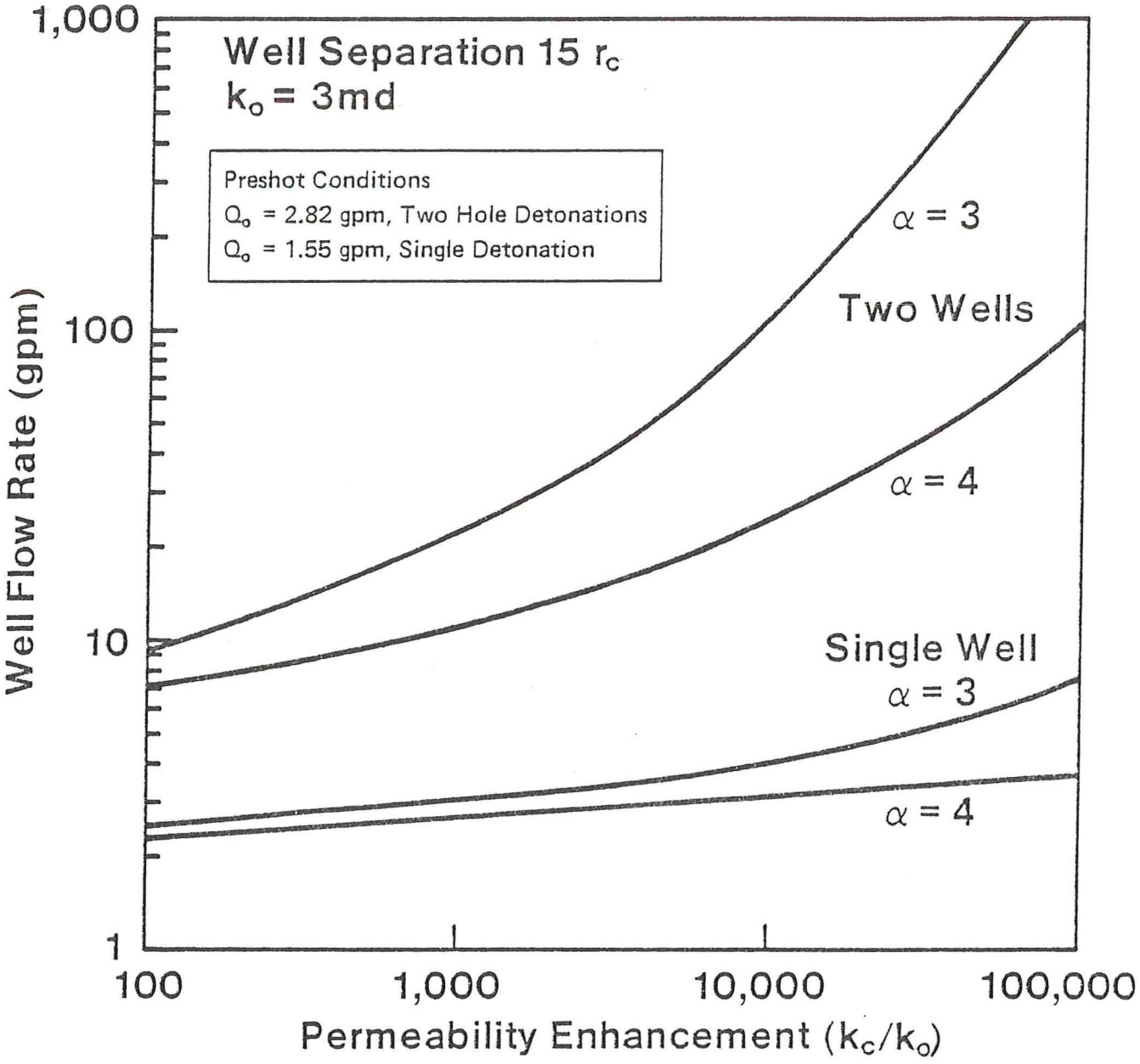

Figure 15.

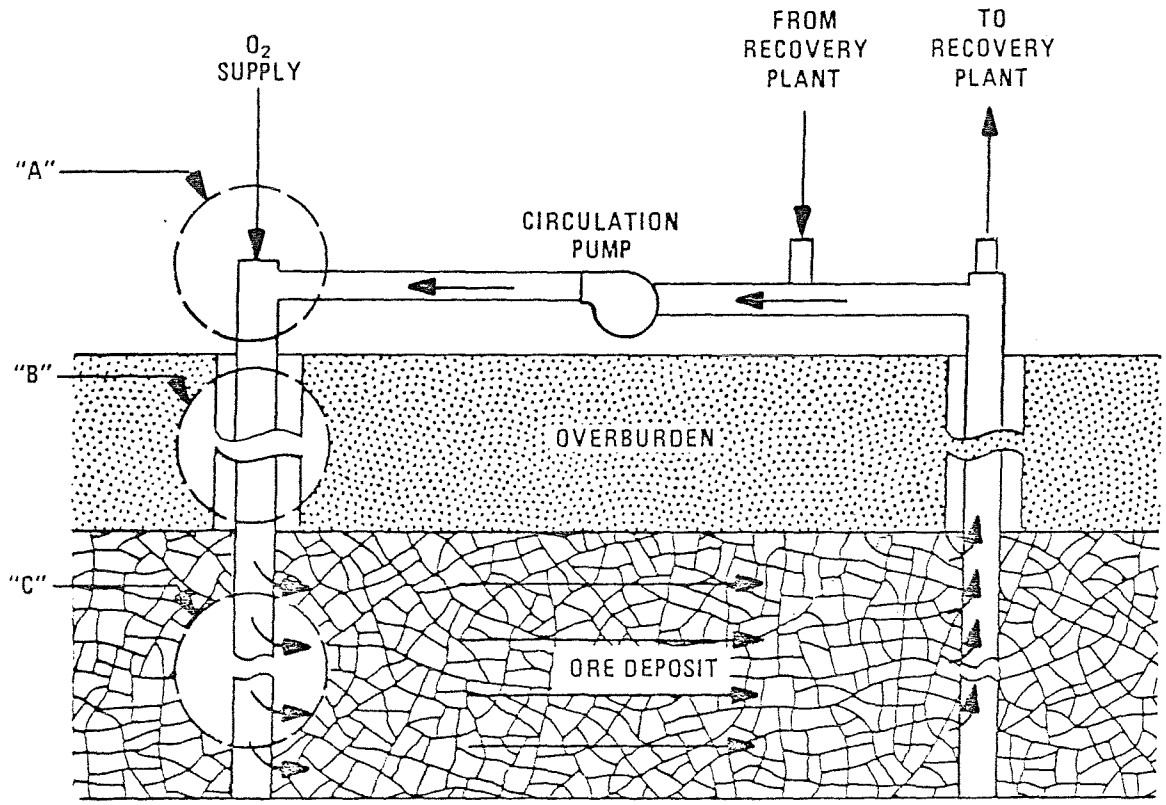

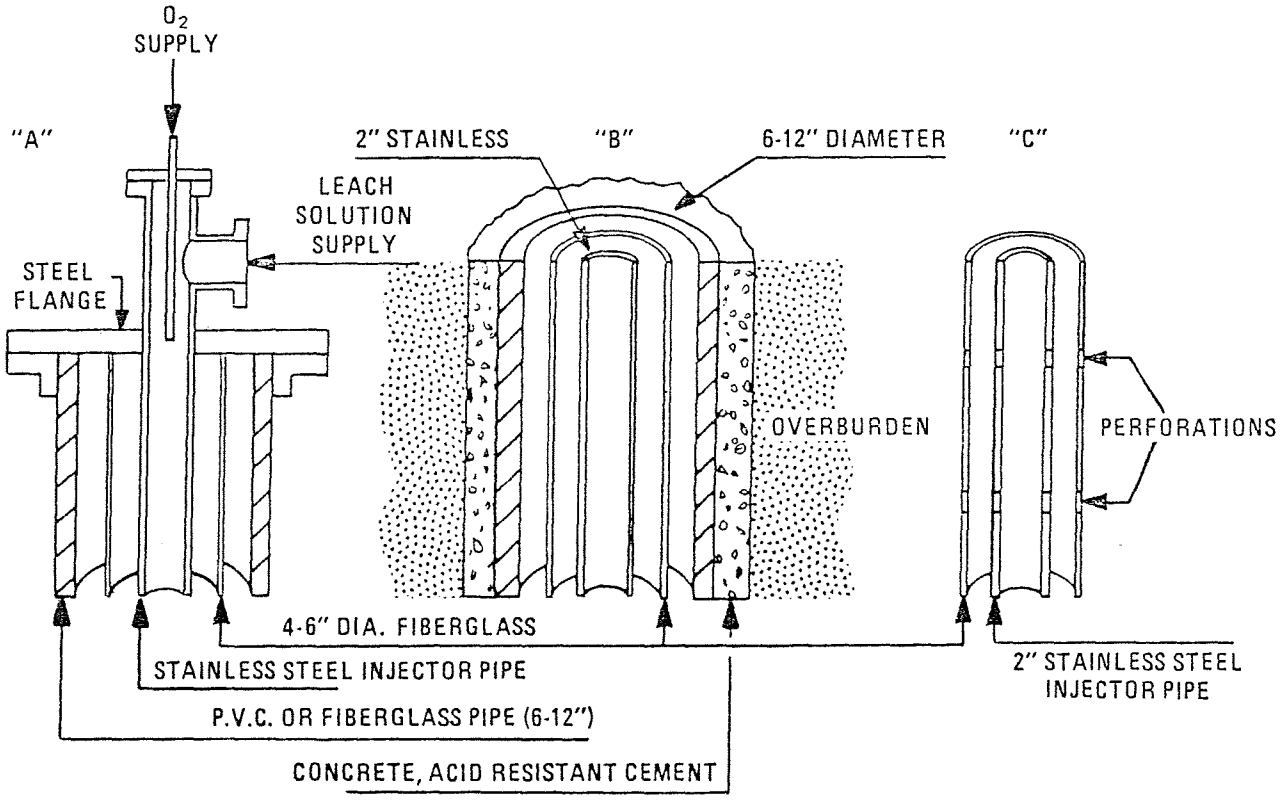

Well Completion

Figure 16.

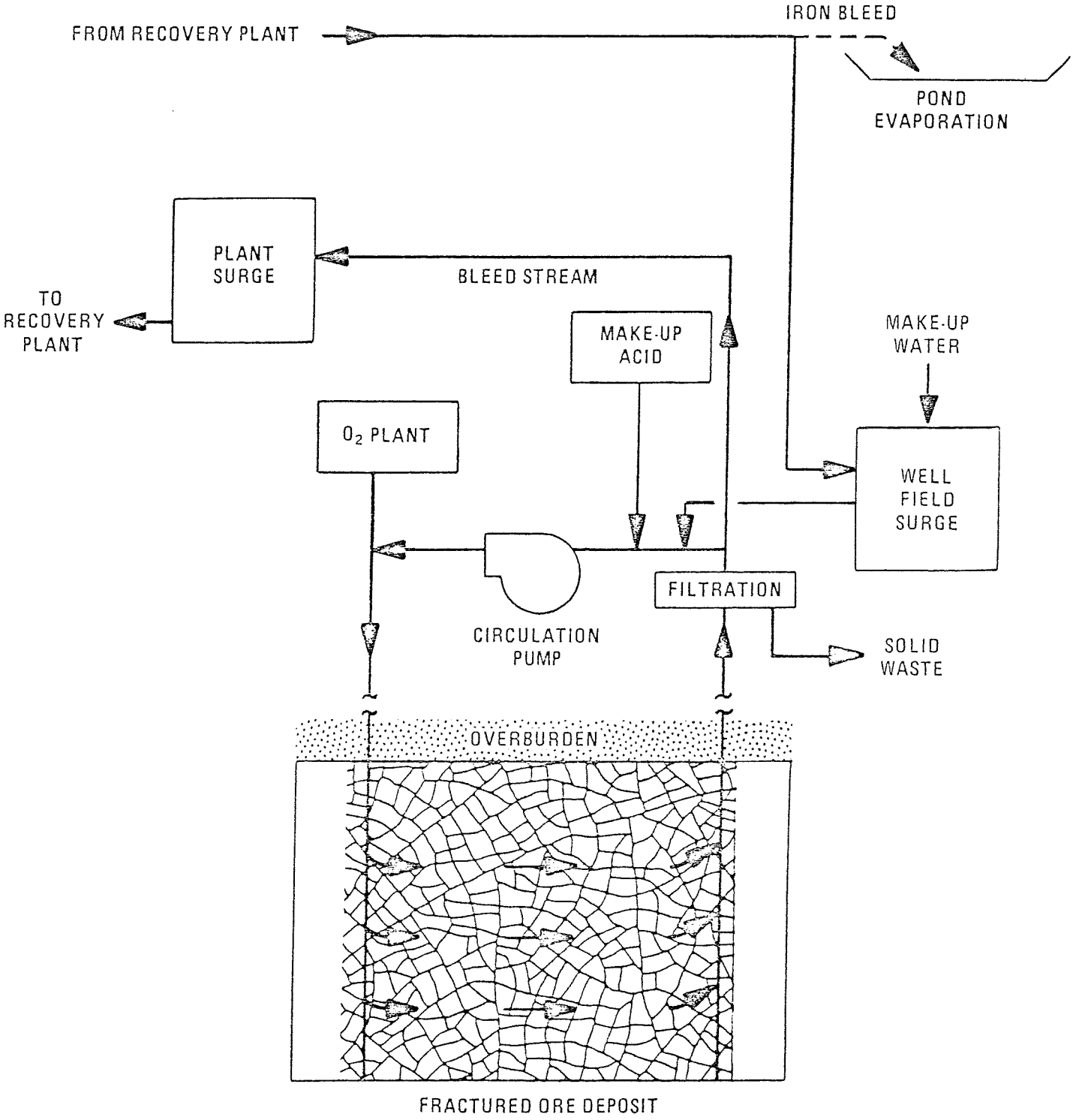

Well Field Pumping Plant

Figure 17.

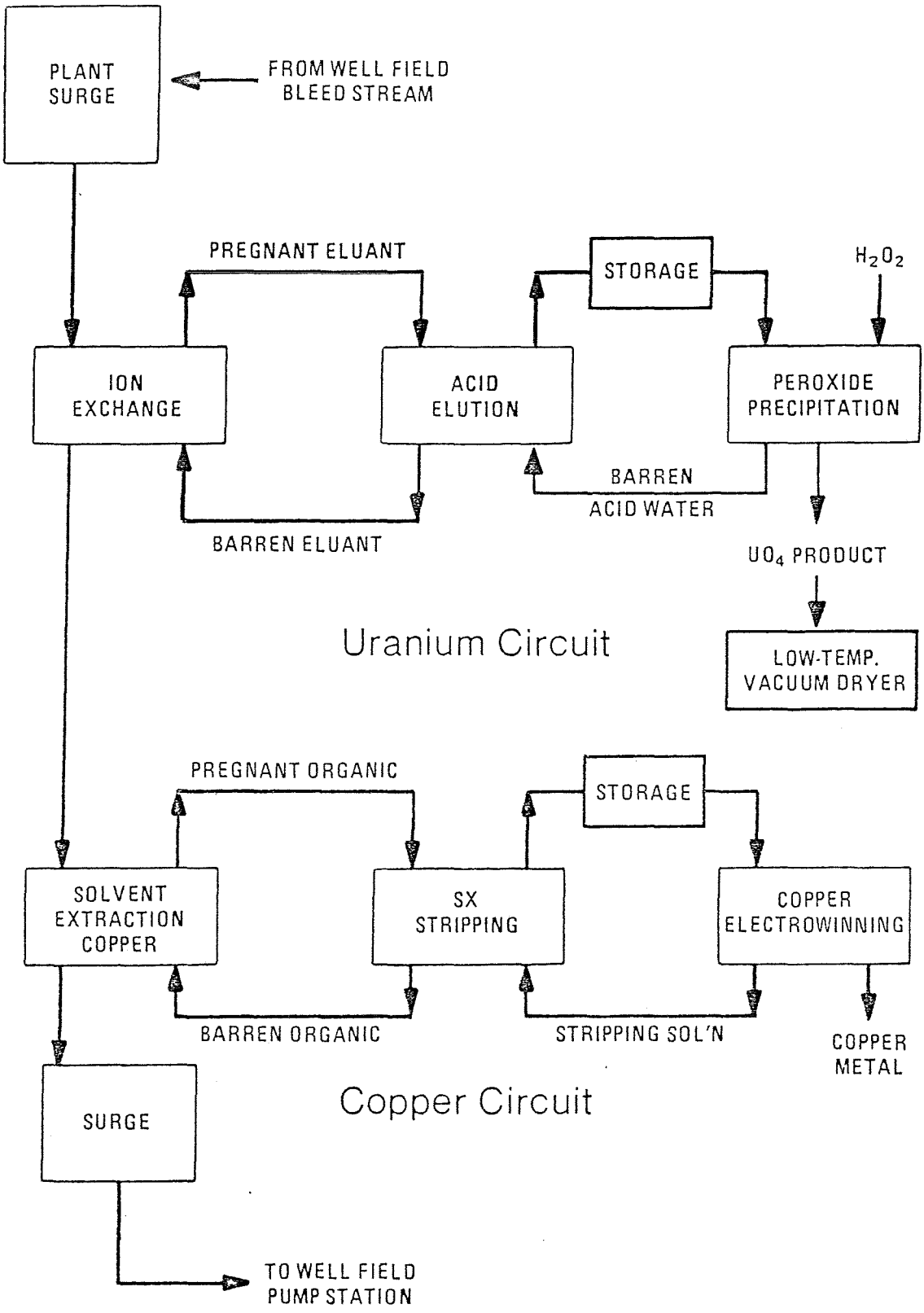

Recovery Plant Flow Diagram

Figure 18.